Minimal Aggregate Size and Minimal Fusion Unit for the First Fusion Pore of Influenza Hemagglutinin-Mediated Membrane Fusion

Joe Bentz
Department of Bioscience and Biotechnology, Drexel University, Philadelphia, Pennsylvania 19104, USA

ABSTRACT The data of Melikyan et al. (*J. Gen. Physiol.* 106:783, 1995) for the time required for the first measurable step of fusion, the formation of the first flickering conductivity pore between influenza hemagglutinin (HA) expressing cells and planar bilayers, has been analyzed using a new mass action kinetic model. The analysis incorporates a rigorous distinction between the minimum number of HA trimers aggregated at the nascent fusion site (which is denoted the minimal aggregate size) and the number of those trimers that must to undergo a slow essential conformational change before the first fusion pore could form (which is denoted the minimal fusion unit). At least eight (and likely more) HA trimers aggregated at the nascent fusion site. Remarkably, of these eight (or more) HAs, only two or three must undergo the essential conformational change slowly before the first fusion pore can form. Whether the conformational change of these first two or three HAs are sufficient for the first fusion pore to form or whether the remaining HAs within the aggregate must rapidly transform in a cooperative manner cannot be determined kinetically. Remarkably, the fitted halftime for the essential HA conformational change is roughly 10^4 s, which is two orders of magnitude slower than the observed halftime for fusion. This is because the HAs refold with distributed kinetics and because the conductance assay monitored the very first aggregate to succeed in forming a first fusion pore from an ensemble of hundreds or thousands (depending upon the cell line) of fusogenic HA aggregates within the area of apposition between the cell and the planar bilayer. Furthermore, the average rate constant for this essential conformational change was at least 10^7 times slower than expected for a simple coiled coil conformational change, suggesting that there is either a high free energy barrier to fusion and/or very many nonfusogenic conformations in the refolding landscape. Current models for HA-mediated fusion are examined in light of these new constraints on the early structure and evolution of the nascent fusion site. None completely comply with the data.

INTRODUCTION

The molecular mechanism by which the envelope glycoprotein hemagglutinin of influenza virus (HA) induces membrane fusion has been intensely studied, because it was the first fusion protein whose structure was solved (Wilson et al., 1981; Bullough et al., 1994). It remains as the paradigm for protein-mediated fusion (Bentz, 1993; Gaudin et al., 1995; Blumenthal et al., 1996; Hernandez et al., 1996; Zimmerberg et al., 1996; Steinhauer et al., 1996; Chernomordik et al., 1998; Weber et al., 1998; Skehel and Wiley, 1998). HA-mediated fusion subsumes at least four distinct intermediates, with a variety of names, subsequent to close apposition of the membranes and the low pH-induced exposure of the HA2 N-terminus (Bentz, 1992; Zimmerberg et al., 1994; Blumenthal et al., 1996; Hernandez et al., 1996; Chernomordik et al., 1997, 1998, 1999; Weissenhorn et al., 1999). Briefly these intermediates are:

1. aggregates of HA formed subsequent to acidification (or perhaps before with the virus, or even the cells), denoted X_j, for a *j*mer of HA trimers. X_ω denotes the minimal aggregate size required to initiate the next step of membrane fusion.
2. the first fusion pore, FP, defined as the first conductivity (2–5 nS) across the membranes. Additional flickering pores usually follow, which lead to the formation of a terminally open pore.[1]
3. the lipidic channel, which is monitored by lipid dye transfer between membranes.
4. the fusion site, which is monitored by aqueous contents mixing (e.g., fluorophors) and the stable joining of the two membranes and complete aqueous contents mixing.

It is generally agreed that the aggregation step precedes the other intermediates. Conductivity flickering, lipid mixing, and then contents mixing usually follow in order (Zimmerberg et al., 1994; Blumenthal et al., 1996), although lipid exchange prior to conductivity has been reported for a particular fluorescent lipid probe (Razinkov et al., 1999).

A rigorous analysis of how HA mediates fusion must begin with the first measurable event. Melikyan et al. (1995) used HA-expressing cells attached to a ganglioside containing planar bilayer to determine the time required for the first fusion pore to form, i.e., the first of the flickering conductivity pores (2–5 nS) from the first of 15–25 attached cells following acidification to pH 4.9. This system monitors the very first destabilization of the planar (target) membrane by

Received for publication 26 October 1998 and in final form 20 October 1999.

Address reprint requests to Joseph Bentz, Drexel University, Department of Bioscience/Biotechnology, 3141 Chestnut St., Philadelphia, PA 19104-2875. Tel.: 215-895-1513; Fax: 215-895-1273; Email: bentzj@drexel.edu.

0006-3495/00/01/227/19 $2.00

[1] The names of the second and third intermediates have been changed from those used in Bentz (1992), due to a better characterization of the process. The first measurable intermediate, called the first fusion pore here, was called an intermembrane intermediate there. The lipidic channel was called a fusion pore there. With these translations, the two works are compatible.

the HAs on the first cell, which requires the fewest reactions for the kinetic model and, hence, allows the most rigorous analysis. Repeating this experiment with fresh planar bilayers yielded a distribution of waiting times (by the cells) for the formation of the first fusion pore. In this work, the subsequent intermediates of the fusion pathway will not be examined, except for a few comments in the discussion.

The current problem in HA-mediated fusion is to correlate the communal intermediates of the fusion process with the well known individual low-pH conformational changes of HA fragments (White and Wilson, 1987; Stegmann et al., 1990; Bullough et al., 1994; Chen et al., 1995; Yu et al., 1994; Hernandez et al., 1996; Carr et al., 1997; Weissenhorn et al., 1999). To understand how the conformational changes of HA generate the kinetic intermediates of fusion, we need to know how many HAs compose the nascent fusion site, i.e., what is the minimal aggregate size (which is denoted ω) required to sustain the subsequent steps of the fusion process. Presumably, only a lower bound for this number can be determined because larger aggregates should also be able to sustain fusion. More importantly, we need to know how many of these HAs in the aggregate must undergo the essential conformational change necessary to create the first fusion pore, i.e., what is the minimal fusion unit (which is denoted q, and obviously $q \leq \omega$).

It is generally believed that the essential conformational change of HA for fusion is to the extended coiled coil. This structure was predicted by Carr and Kim (1993), proven for a soluble fragment of HA by Bullough et al. (1994), and morphologically observed by Shangguan et al. (1998) on the intact virus. Qiao et al. (1998) found that mutations predicted to hinder the extended coiled coil formation did inhibit fusion. However, because neither kinetics nor site directed mutagenesis can prove that the formation of the extended coiled coil is the essential conformational change, nor has this been proven yet by a structural technique, it is prudent to use the term essential conformational change to signify this kinetically identified event.

The minimal aggregate size (ω) and the minimal fusion unit (q) are both essential and fundamentally distinct parameters of fusion. They must be fitted separately. The model can ascertain the value of how many HAs (denoted q) must transform at a slow rate before the fusion pore forms, where $q \leq \omega$. If $q < \omega$, as will turn out to be the case, there are two possibilities: 1) it is sufficient that only q HAs within the aggregate transform to cause the formation of the first fusion pore, while the remaining HAs may have another function; or 2) the remaining HAs in the aggregate transform rapidly in a cooperative process. These two possibilities are kinetically identical, but mechanistically quite different. If there is cooperativity, then the structure of the nascent fusion site must substantially change to induce a cooperativity, which will not be rate-determining for fusion. To prove cooperativity, some other means of measuring how many HAs transformed rapidly would be required. A third possibility, that after a few have transformed the remaining HAs transform even more slowly, is simply a kinetic subset of the second case, because the first few fast transformations would not be kinetically observed. The value of q would be well estimated and ω would be decremented by the value of q, which is not serious because we can only underestimate ω already.

Previous work attempted to determine how many HAs are at the fusion site. Ellens et al. (1990) used the fusion of glycophorin-bearing liposomes with two HA-expressing cell lines (the same as used by Melikyan et al., 1995), with a roughly twofold difference in HA surface density to show that more than one HA was required at the fusion site, i.e., $\omega \geq 2$. Danieli et al. (1996) monitored the lipid mixing between erythrocyte ghosts with several HA-expressing cell lines (with about a 10-fold difference overall in HA surface densities). They used a Hill type equation to analyze lag times and initial rates of lipid mixing and claimed that 3–4 HAs were required for the cooperative step. This analysis has no rigorous theoretical basis, as discussed by Blumenthal et al. (1996). In addition, Blumenthal et al. (1996) monitored a membrane potential shift, the lipid mixing and the contents mixing between erythrocyte ghosts and cells from a single HA-expressing cell line. They fit their data for the kinetics of fusion site formation using an empirical equation based upon pore opening kinetics. They claimed that six HA trimers formed the fusion site. This data analysis is superior to that of Danielli et al. (1996) in that the entire time course was fitted, but, without the comparison of at least two HA surface densities, their fitted parameters remain empirical.

When the mass action model proposed here is used to analyze the data of Melikyan et al. (1995), we find that the minimal aggregate size for the formation of the first fusion pore is at least $\omega \geq 8$ HAs, and it could be substantially larger. This relatively large number of HAs fits well with the model of HA aggregation proposed by Kozlov and Chernomordik (1998), which begins with insertion of the HA fusion peptide into the viral envelope (or HA-expressing cell membrane). Remarkably though, we find that only $q = 2$ or 3 of these HAs need to undergo the essential conformational change slowly before the first fusion pore forms. This leads to an intriguing pair of questions. If the remaining HAs transform rapidly, such that there is a cooperative unit of the order of at least 6, then how does the nascent fusion site change to induce cooperativity? If, in contrast, only two or three HAs need to transform to create the first fusion pore, then how does this happen and what might be the function of the other HAs in the aggregate? These questions will be addressed in the Discussion.

THE MASS ACTION MODEL

Constructing a useful mass action model for HA mediated fusion, with the smallest number of physically meaningful

parameters, begins with deciding which steps are kinetically significant. There is only evidence for two conformations for HA after acidification: the fusion peptide exposed and the extended coiled coil. The exposure of the fusion peptide from HA following the pH acidification is very rapid compared with fusion kinetics (White and Wilson, 1987; Stegmann et al., 1990; Bentz, 1992; Pak et al., 1994), so this is not a kinetically significant step. The rate of formation of the extended coiled coil is not known from structural studies, but cryoelectron micrographs of PR8 virus suggest a halftime on the order of 10^3–10^4 s (Shangguan et al., 1998). Although the close approach of another membrane could alter the kinetics of the coiled coil formation, it is likely for those HAs bound to target membrane sialiosides that the conformational change would be slower, rather than faster (Ellens et al., 1990; Alford et al., 1994). Other conformations preceding the formation of the extended coiled coil could be postulated, but their necessity remains to be demonstrated. Here we will consider only one conformational change subsequent to low pH-induced exposure of the fusion peptide, i.e., the essential one for the formation of the first fusion pore, which is expected to be to the extended coiled coil (Bullough et al., 1994; Carr et al., 1997; Qiao et al., 1998; Shangguan et al., 1998; Skehel and Wiley, 1998).

There are only two simple kinetic models for relating the aggregation of HAs to the formation of the first fusion pore. The first postulates that exposure of the fusion peptides causes rapid HA aggregation, and the rate-limiting step for fusion is the essential conformational change of the HAs within an aggregate (Bentz, 1992; Kozlov and Chernomordik, 1998). The mechanism of rapid HA aggregation could be adhesion of the amphiphilic fusion peptides in the aqueous space (Ruigrok et al., 1988), or by membrane curvature minimization due to fusion peptides embedded in their own (viral or HA-expressing cell) membrane (Kozlov and Chernomordik, 1998), or by other interactions.

The second kinetic model postulates that the rate of fusion pore formation would be limited by the aggregation of HAs that have already undergone the essential conformational change. This kinetic model has never been analyzed, but is implicitly contained within most published models, e.g., Hernandez et al. (1996), Carr et al. (1997), Chernomordik et al. (1998) and Skehel and Wiley (1998). Aggregation of HAs that have not yet undergone the essential conformational change would not be relevant. Other, more complex, models can be constructed, but these two are the simplest.

In Appendix B, we will see, at first glance, that these two models appear to yield similar equations. However, the slow aggregation of activated HAs (the second model) cannot fit the data of Melikyan et al. (1995) for both cell lines simultaneously with consistent parameters in any simple way. The basic problem is that the HA aggregation rate-limited fusion model depends only upon the size of the aggregate of activated HAs and, so, it fails to provide separate parameters for the number of fusogenic aggregates (which would depend upon the HA surface density and the minimal fusogenic aggregate size, ω) and for the number of HAs within an aggregate that must undergo the essential conformational change, i.e., q. The data strongly prefers separate parameters. Plonsky et al. (1999) have argued that the rate-limiting step in baculovirus GP64 fusion pore formation was not aggregation of GP64.

Although a more complicated kinetic scheme could probably fit the aggregation rate-limited fusion model to the data of Melikyan et al. (1995), simplicity and other data favor a model wherein HA aggregation is rapid and the fusion intermediates form as a consequence of a slow and essential conformational changes of HA. Related data include that the lateral mobility and mobile fraction of HA on cells is consistent with rapid HA aggregation (Ellens et al., 1990; Bentz, 1992; Melikyan et al., 1995; Danieli et al., 1996). The model of Kozlov and Chernomordik (1998) would predict rapid and reversible HA aggregation. In Appendix A, it is shown that, even if only one out of ten HA collisions leads to aggregation, either before or following low pH, then HA aggregation would be at equilibrium well before fusion begins. On virions, it could be that the HA packing is close enough to qualify as preaggregated even before acidification.

Bentz (1992) derived kinetic equations for the evolution of the fusion intermediates described above to illustrate some of the traps encountered by trying to use initial rates, Arrhenius plots and/or lag times to decipher the number of HAs (ω) required at the fusion site or the activation energy of the process. The inescapable conclusion was that to determine the value of the number of HAs required at the fusion site required that fusion kinetics be measured as a function of HA surface density. The essential conclusions reached in that work are unchanged by the revised mass action model given here. However, the equations derived in Bentz (1992) assumed, for simplicity and in the absence of data, that the first fusion pore formed in a concerted fashion from the ωmer aggregate, i.e., $q = 0$. The resultant equation for the formation of the first fusion pore (derived from Eq. 6 in Bentz (1992) for the first fusion pore[Footnote 1]) is a hyperbolic curve that cannot fit the sigmoidal data of Melikyan et al. (1995) presented here. Thus, the model given in Bentz (1992) must be expanded.

Initially, we assume that this conformational change can happen independently and identically for any HA in the ωmer aggregate. The mass action reaction for this process is

$$X_{\omega,0} \underset{k_{rf}}{\overset{\omega k_f}{\rightleftharpoons}} X_{\omega,1} \underset{2k_{rf}}{\overset{(\omega-1)k_f}{\rightleftharpoons}} \cdots X_{\omega,\mathrm{q}-1} \underset{q\,k_{rf}}{\overset{(\omega-(q-1))k_f}{\rightleftharpoons}} X_{\omega,\mathrm{q}}, \qquad (1)$$

where $X_{\omega,\mathrm{j}}$ denotes an aggregate of ω HAs, of which j HAs have undergone the essential conformational change and $\omega - j$ HAs are still in the low pH/fusion peptide-exposed configuration. k_f denotes the rate constant at which any

identical and independent HA trimer undergoes the essential conformational change, so that an aggregate of ω HAs would have an overall rate of ωk_f for the first change within the aggregate and $(\omega - 1)k_f$ for the second change within the aggregate, et cetera. $[X_{j,o}\ (t = 0)]$ is the initial surface concentration of HA $j$mers, i.e., just after acidification induces the aggregation to the equilibrium distribution, but before any subsequent membrane destabilization steps have occurred. For generality, k_{rf} denotes the rate at which any HA trimer undergoes the reversal of the essential conformational change. Without evidence that this first conformational change is significantly reversible, which seems unlikely, we will henceforth assume that $k_f \gg k_{rf}$, which will not affect the basic structure of the kinetic equations or their solutions.

Although we assume that, initially, each of the ω HAs in the fusogenic aggregate undergo the essential conformational change at the same rate, that does not mean that all of them must do so for the first fusion pore to form. With oxygen dissociation from hemoglobin, each of the four bound oxygens are essentially identical initially, but once the first oxygen dissociates slowly, the remaining oxygens dissociate rapidly. Cooperativity in this case refers to the simultaneous departure of the last three (or so) oxygens. After q of the HAs in the ωmer have undergone the essential conformational change slowly, the remainder might rapidly and cooperatively transform, yielding the first fusion pore. Alternatively, perhaps only q the HAs in the ωmer need to transform to form the first fusion pore, whereas the remaining untransformed HAs could be either redundant or they could play another role in the destabilization mechanism.

Thus, we have introduced a second parameter, denoted q, to indicate how many of the HAs in the aggregate must undergo the essential conformational change at the rate k_f, which is the reaction series shown in Eq. 1. It is clear that q is actually the more crucial parameter to know for understanding the molecular mechanism of the fusion reaction. The actual number of HAs in the fusion site appears less important, unless the untransformed HAs actually have a function in the fusion mechanism.

The first fusion pore forms, either because having q HAs transform is adequate or because the remaining $(\omega - q)$ HAs transform rapidly. These two possibilities are kinetically the same, so that the next mass action reaction can be written as

$$X_{\omega,q} \xrightarrow{k_p} \mathrm{FP}. \tag{2}$$

The subsequent reactions to other intermediates are not germane to the data being analyzed here, because only the time required for the formation of the first fusion pore is being fitted, which is independent of the subsequent reactions.

It seems likely that, if an ωmer aggregate can support fusion, then so can higher order aggregates. However, the kinetic analysis of the higher order aggregate's contribution to fusion is not simple, because there is no simple analytical model of HA aggregation. Nevertheless, their contribution will be estimated here through the analysis of extreme cases. Assuming that aggregates larger than ωmers can support fusion, we can write the mass action kinetic equations for these reactions from any $\omega + j$-mer (for $j \geq 0$ and $i < q$) leading to the first fusion pore formation (ignoring back reactions) as

$$\begin{aligned}
\frac{d[X_{\omega+j,0}]}{dt} &= -(\omega + j)k_f[X_{\omega+j,0}] \qquad (3)\\
&\vdots\\
\frac{d[X_{\omega+j,i<q}]}{dt} &= -(\omega + j - i)k_f[X_{\omega+j,i}]\\
&\quad + (\omega + j - (i-1))k_f[X_{\omega+j,i-1}]\\
\frac{d[X_{\omega+j,q}]}{dt} &= -k_p[X_{\omega+j,q}]\\
&\quad + (\omega + j - (q-1))k_f[X_{\omega+j,q-1}]\\
\frac{d[\mathrm{FP}]}{dt} &= k_p \sum_{j=0}[X_{\omega+j,q}].
\end{aligned}$$

The summation is finite because the number of HAs is finite and ends when the number of $X_{\omega+j,q}$ aggregates within the area of apposition falls below one. Approximate and numerically integrated solutions to these equations will be given below, providing the mass action concentrations of these fusion intermediates on the average cell surface.

The conductivity change will be measured if the cell has one or more than one fusion pores. In contrast, even if the average number of fusion pores over the whole ensemble is one, a randomly chosen cell need not yet have one. To estimate the fraction of cells that have a first fusion pore, which is what Melikyan et al. (1995) measured, we first need to know the average number of first fusion pores within the area of apposition. This is equal to $[\mathrm{FP}(t)]$ times the area of apposition between the cell and the bilayer, which is denoted δ. This area δ is simply a rough estimate of the area of apposition. δ can range from about ⅓ of the cell surface area (where the cell sits like a hemisphere on the planar bilayer) to about ½ of the cell surface area (where the cell is essentially flattened on the planar bilayer). Possible microinvaginations would be impossible to measure reliably under the experimental conditions and they probably would not significantly affect the number of HAs in the area of apposition because the HAs are very mobile (Ellens et al., 1990; Danielli et al., 1996). Furthermore, the parameters of

the fits are not very sensitive to the choices within this range, as shown in the Results.

Now, the fraction of cells with one or more first fusion pores is equal to the probability that a randomly chosen cell will have at least one first fusion pore and is given by the binomial distribution. Because there are more than 25 points (i.e., cells monitored) in each data set analyzed, the Poisson form is less cumbersome (Bentz, 1992):

$$N_p(t) = 1 - \exp\{-\delta[\mathrm{FP}(t)]\}. \tag{4}$$

$N_p(t)$ is the function we will be fitting to the data of Melikyan et al. (1995), using both the numerically integrated value of [FP(t)] from Eq. 3, and the approximate Eq. 8 derived below.

APPROXIMATE SOLUTIONS FOR THE MASS ACTION KINETICS

The differential equations given above will be numerically integrated, but first we will develop an approximate solution that is simple and sufficiently accurate to uncover the most important information contained in the data. To begin, for $i < q$, the surface concentrations of the HA ωmers that have i HA trimers that have undergone the essential conformational change are given by the binomial formula,

$$\begin{aligned}[X_{\omega+j,i}(t)] &= [X_{\omega+j,0}(0)]\frac{(\omega+j)!}{(\omega+j-i)!\,i!}(1-\exp\{-k_f t\})^i \\ &\quad\times(\exp\{-k_f t\})^{\omega+j-i} \\ &\approx [X_{\omega+j,0}(0)]\frac{(\omega+j)!}{(\omega+j-i)!\,i!}(1-\exp\{-k_f t\})^i.\end{aligned} \tag{5}$$

Here we are only concerned with the formation of the first fusion pore, so very few HAs are going to be consumed by the fusion process. In general, $k_f t \ll 1$ when the first fusion pore forms, so that $\exp\{-(\omega + j - i)k_f t\} \approx 1$, and was so replaced in Eq. 5 for convenience below. For $i = q$, the surface concentrations are given by

$$\begin{aligned}&[X_{\omega+j,q}(t)] \\ &= k_f(\omega+j-(q-1))e^{-k_p t}\int_0^t e^{+k_p u}[X_{\omega+j,q-1}(u)]\,du \\ &\approx \frac{(\omega+j)!}{(\omega+j-i)!\,i!}[X_{\omega+j,0}(0)] \\ &\quad\times\left\{k_f q e^{-k_p t}\int_0^t e^{+k_p u}(1-\exp\{-k_f u\})^{q-1}\,du\right\},\end{aligned} \tag{6}$$

using Eq. 5.

It can be shown (within the spirit of obtaining a simple approximate equation) that

$$\begin{aligned}[\mathrm{FP}(t)] &= k_p\int_0^t \sum_{j=0}[X_{\omega+j,q}(s)]\,ds \\ &\approx \left\{k_f q\int_0^t (1-\exp\{-k_f u\})^{q-1}(1-\exp\{-k_p(t-u)\})\,du\right\} \\ &\quad\times\left(\sum_{j=0}\frac{(\omega+j)!}{(\omega+j-q)!\,q!}[X_{\omega+j,0}(0)]\right) \\ &\approx \{(1-\exp\{-k_f t\})^{q+1}\} \\ &\quad\times\sum_{j=0}\frac{(\omega+j)!}{(\omega+j-q)!\,q!}[X_{\omega+j,0}(0)],\end{aligned} \tag{7}$$

where Eq. 6 was used and the order of integration is reversed. The final approximation for the integral equation in the braces assumed that $\exp\{-k_p t\} \ll 1$ and is to first order to obtain rough estimates for q and k_f. It is most accurate when $2 \le k_p/k_f \le 10$, which is the domain of greatest interest.

We now have an approximate solution for the average surface density of first fusion pores on the HA-expressing cells, on the surface closely apposed to the target membrane, which is the planar bilayer for the data of Melikyan et al. (1995). When Eq. 7 is used for the average surface density of first fusion pores per cell, then the average number of cells with one or more fusion pores is given by Eq. 4 as

$$N_p(t) \approx 1 - \exp\{-A(1-\exp\{-k_f t\})^{q+1}\}, \tag{8}$$

$$A \equiv \delta\sum_{j=0}\frac{(\omega+j)!}{(\omega+j-q)!\,q!}[X_{\omega+j,0}(0)].$$

The amplitude factor A has absorbed the imprecise information about the HA aggregate surface density dependence and the area of apposition. A equals the total number of fusogenic units, or q-lets, within the area of apposition. It will be seen that this equation provides a good approximation for the numerical integrations.

Clearly, the approximate Eq. 8 will yield relatively unambiguous estimates for k_f and q. However, the estimate for ω, the minimal aggregate size of HAs comprising a nascent fusion site, will depend upon the details of the aggregation equilibrium and must be extracted from the fitted value of A, which is why more than one HA surface density much be used to estimate ω (Bentz, 1992). The smallest estimate for ω can be obtained by assuming that the aggregation process occurs by nucleation, i.e., only ωmers can coexist with the HA, and the definition of the amplitude factor A contains only the $j = 0$ term. This way, no HAs are wasted in

unproductive/unfusogenic aggregates or aggregates with more HAs than necessary to sustain the first fusion pore. As shown in Appendix A, for cells with different amounts of HA per cell (e.g., GP4f and HAb2, which was used by Melikyan et al., 1995), the ratio of their amplitude factors A obtained from the approximate fit give an underestimate of the lower bound for ω as

$$\frac{[\mathrm{HAb2}]}{[\mathrm{GP4f}]} < \frac{A(\mathrm{HAb2})/\delta(\mathrm{HAb2})}{A(\mathrm{GP4F})/\delta(\mathrm{GP4f})} < \left(\frac{[\mathrm{HAb2}]}{[\mathrm{GP4f}]}\right)^{\omega}$$

$$\Rightarrow \omega > \ln\left\{\frac{A(\mathrm{HAb2})}{A(\mathrm{GP4f})}\Big/\frac{\delta(\mathrm{HAb2})}{\delta(\mathrm{GP4f})}\right\}\Big/\ln\left\{\frac{[\mathrm{HAb2}]}{[\mathrm{GP4f}]}\right\}, \quad (9)$$

where [HAb2] and [GP4f] denotes the initial surface densities of HA on the HAb2 and GP4f cell lines, respectively. δ(HAb2) and δ(GP4f) denote the area of apposition for the two cell lines, which are not the same because the cell lines have different average surface areas (Ellens et al., 1990). The inequality is a general result from aggregation models (Bentz and Nir, 1981a,b), which asymptotically reach equality as the HA surface densities approach zero. In Appendix A, Eq. A7, a more reasonable analysis of aggregation would yield an estimate for ω larger than that predicted by Eq. 9. The analysis also shows that the ratio of the amplitude factors A(HAb2)/A(GP4f) obtained by the approximate Eq.8 must be achieved using the exact calculations and whatever the aggregation model for HA. This is an important conclusion from the approximate analysis.

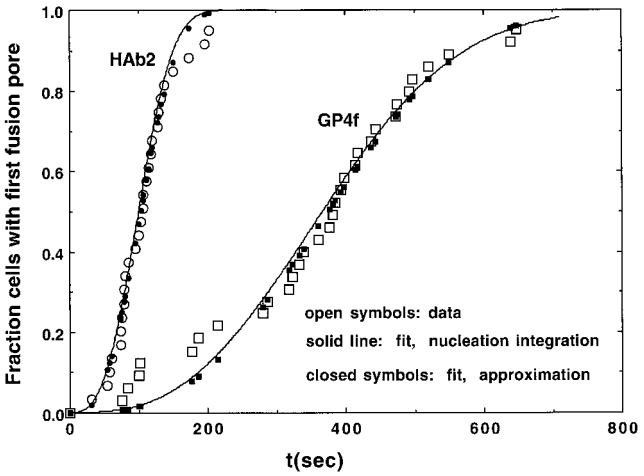

FIGURE 1 The open symbols are the data from Melikyan et al. (1995) showing the cumulant fraction of cells that have achieved their first conductivity channel across the planar bilayer (i.e., the formation of the first fusion pore) as a function of time. The bilayer was composed of dioleoylphosphatidylcholine/bovine brain phosphatidylethanolamine in the ratio 2:1, with 5 mol% gangliosides, equal weights of GD1a and GT1b, added. The cells were prebound to the planar bilayers before acidification. The HAb2 cells (*open circles*) required about 100 s for half of the cells to achieve their first conductivity channel, whereas the GP4f cells (*open squares*) required about 360 s. The solid symbols come from using the approximate equation for $Np(t)$, Eq. 8, using $k_f = 1.5 \times 10^{-4}\ s^{-1}$, $q = 1.9$, and Eq. 10. The solid lines show a typical best fit for the numerical integration, Eqs. 3 and 4, with the nucleation model using $\omega = 8$, $q = 2$, $k_f = 1 \times 10^{-4}\ s^{-1}$, and $k_P = 2.5 \times 10^{-4}\ s^{-1}$, and the number of fusogenic aggregates within the area of apposition for the GP4f cell line N_ω(GP4f) = 680 and for the HAb2 cell line N_ω(HAb2) = 27,880, using Eqs. 3 and 4.

RESULTS

Melikyan et al. (1995) bound roughly 15–25 HA-expressing cells at 35–37°C to a horizontal planar bilayer (containing 5 mol% gangliosides, with equal weights of gangliosides GD1a and GT1b, as the sialoside receptor for HA1), lowered the pH to 4.9, and measured the time required for the first cell on the planar bilayer to establish the first conductivity channel, i.e., the first fusion pore. This protocol was then repeated with a fresh planar bilayer to obtain a waiting time for the first fusion pore for the next set of 15–25 cells, and so on. They used two cell lines expressing different HA surface densities. The HAb2 cell line expressed between 1.9 (Ellens et al., 1990) and 1.6 (Danieli et al., 1996) more HA/μm^2 on the cell surface than did the GP4f cell line, which had roughly 3×10^6 HAs/GP4f cell (Ellens et al., 1990). This ratio was not measured by Melikyan et al. (1995).

The open symbols in Fig. 1 are the data from Melikyan et al. (1995) showing the cumulative fraction of cells that have achieved their first conductivity channel across the planar bilayer (i.e., the formation of the first fusion pore) as a function of time. The original waiting time data was converted to a cumulative fraction by normalizing the data point with the longest waiting time to represent 0.95 of the cells. This was done because the model can only reach a fraction of 1 after an infinite length of time. Normalizing to 0.99 or 0.9 made no significant difference to the fitting or the predicted parameters.

The HAb2 cells (*open circles*) required about 100 s for half of the cells to achieve their first conductivity channel, whereas the GP4f cells (*open squares*) required roughly 360 s. Using the same cell lines several years earlier, Ellens et al. (1990) found that 4.4 times more glycophorin-containing liposomes ($\approx$1 μm diameter) fused eventually to the HAb2 cells (one liposome fusing out of 75 bound) than to the GP4f cells (one liposome fusing out of 330 bound) following a 90-s incubation at low pH. Given the difference in assays and the passage of time, the overall agreement is quite good.

The closed symbols and lines in Fig. 1 represent fittings from the approximate and exact equations, respectively. We will start the fitting of the data using the approximate solution for $N_p(t)$ from Eq. 8, to determine the general properties of the system. In particular, there are four parameters that must be fitted: k_f, q, A(GP4f), and A(HAb2), which actually is the minimum number needed to fit two sigmoidal curves. The same values of k_f and q must be used for both cell lines, whereas the amplitude factors, A(HAb2)

and A(GP4f), will be fitted for each cell line. The minimal value of ω will be obtained from the ratio of A(HAb2)/A(GP4f), using Eq. 9. We used the fitting routine of MATLAB (fmins, The Math Works, Natick, MA), which is unconstrained and which minimized the root mean square error between the data points and the calculated value of $N_p(t)$ for both cell lines simultaneously.

The fits to the approximate Eq. 8 were very sensitive to the value of q, with marked deterioration when q deviated from the range of 1.9 ± 0.1. With $q = 1.9$, there were several distinct sets of values for A(HAb2), A(GP4f), and k_f that could fit the data equally well. However, for all of the best fits (rmse $< 3.9 \times 10^{-2}$), the fitted values of A(HAb2) and A(GP4f) were strongly correlated with the value of k_f, which is shown in Fig. 2. The following correlation equations were obtained from Fig. 2 using those fits for $k_f > 1e^{-5}$ s^{-1}, which was the physically relevant regime, as will be explained below:

$$A(\text{GP4f}) = 10^{-2.6}/(k_f^{2.8}), \tag{10}$$

$$A(\text{HAb2}) = 40A(\text{GP4f}).$$

Just below, and in Appendix B, we shall see why A(GP4f) should be correlated with k_f.

To further analyze these fitted parameters, it is necessary to estimate the area of apposition between the cell and the planar bilayer. Ellens et al. (1990) used whole-cell capacitance to estimate cell surface areas and found that the HAb2 cells had roughly 40% more plasma membrane on average than the GP4f cells. There is no experimental reason to believe that these cells differ in any property other than gross size and HA surface density (Ellens et al., 1990; Melikyan et al., 1995; Danieli et al., 1996), so we will assume that the same fraction of cell surface is in close apposition to the planar bilayer for both lines. This area will be between a half (for a very flattened cell) to a third (for a hemispherical cell) of the total cell surface area. Visual estimates of cell flattening roughly yield $\delta = ⅓$ of the cell surface is in apposition with the planar bilayer (G. Melikyan, personal communication). Because the HAb2 cells are larger, this affords them a comparatively larger area of apposition. Choosing $\delta = ½$ would only slightly affect the parameter estimates. So, the relative surface areas of the cells is δ(HAb2)/δ(GP4f) $\approx$ 1.4, assuming that the cells bind equivalently (i.e., ⅓ of their total surface area) to the planar bilayer.

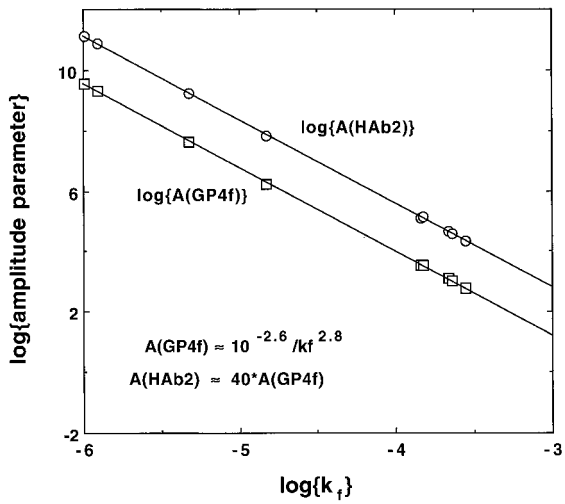

FIGURE 2 The correlation of the value of fitted value of k_f with the fitted parameters A(HAb2) and A(GP4f), obtained using the approximate solution Eq. 8. The slopes of the lines are given in Eq. 10, from those data for $k_f > 1e^{-5}$ s^{-1}, which was the physically relevant regime, as explained in the results.

The ratio of A(HAb2)/A(GP4f) $= 40 \pm 2$ for all best fits. Eq. 9 then yields $\omega > \log\{40/1.4\}/\log\{1.6 \text{ to } 1.9\} = 5.2$ to 7.1, where the variation is due to the uncertainty in the relative HA surface densities, i.e., 1.9 (Ellens et al., 1990) to 1.6 (Danieli et al., 1996). In Appendix A, it is shown that the minimal aggregate size could be substantially larger.

The fitted values of k_f had to be smaller than 2×10^{-4} s^{-1}, otherwise the fits deteriorated markedly, rmse $> 3.9 \times 10^{-2}$. The value of k_f could decrease as long as the amplitude factors A could increase, as described in Eq. 10. This result is simply an asymptotic outcome of monitoring only the first fusion pore, so that $k_f t \ll 1$ in Eq. 8 and $N_p(t) \rightarrow 1 - \exp\{-A(k_f t)^{q+1}\}$ in this limit, see Appendix B.

However, k_f had to be larger than 1×10^{-5} s^{-1}, otherwise the predicted values for A(HAb2) from Eq. 8 would require more than the total number of HAs on the cell surface, which is clearly impossible. There are roughly 3×10^6 HAs on the GP4f cells and 7×10^6 on the HAb2 cells (Ellens et al., 1990; Danieli et al., 1996). The lower bound for k_f follows directly from Eq. 10 and the definition of the amplitude factor A in Eq. 8 by noting that the number of ωmer aggregates in the area of apposition for the HAb2 cells must be less than $7 \times 10^6/(3\omega)$, which is a very conservative estimate, together with $\omega = 8$, $q = 2$, and $\delta = ⅓$ of the cell surface area. This can be considered as a greatest lower bound for the value of k_f. Thus, k_f is estimated to be within a fairly small range of values. The solid lines in Fig. 1 show the fits for the approximate Eq. 8 with $k_f = 1.5 \times 10^{-4}$ s^{-1}, $q = 1.9$ and Eq. 10 above.

Given this preview of the parameters from the approximate fitting, we now turn to the more rigorous fitting of the data by Eq. 4 using the numerical integration of Eq. 3 (using MATLAB subroutine ODE23, The Math Works). We will primarily consider the nucleation model, i.e., only ωmers could be formed from the HAs, as described in Appendix A, because it introduces no new parameters into the fit. The nucleation model allows no aggregates smaller than that capable of sustaining fusion, i.e., an ωmer, and so provides the maximal increase in the density of ωmers for an increase in HA surface density. It also allows no aggregates larger than ωmers, which, although (presumably) fusogenic,

would waste HAs. Therefore, it will predict the smallest value of ω for the minimal fusogenic aggregate size relative to all other aggregation models.

Using this nucleation model, the protocol is straightforward. For given values of ω and q, the data is fitted for k_f, k_p, and the initial number of fusogenic ωmer aggregates in the area of apposition for the GP4f cell line, $N_\omega(\text{GP4f}) = \delta[X_{\omega,0}(t = 0), \text{GP4f}]$, and for the HAb2 cell line, $N_\omega(\text{HAb2}) = \delta[X_{\omega,0}(t = 0), \text{HAb2}]$. The relative cell sizes and apposition areas are not needed for the fit. They are needed to determine which of the fits require more HA than is physically available, i.e., as k_f and k_p become smaller, larger values of N_ω(GP4f) and N_ω(HAb2) are needed to fit the data. Eventually more HA is required than is available, just as with the approximate fits. As with the approximate solution, many sets of parameters could fit the data. It was found that simulated data was fitted uniquely and correctly by the fitting routine for several representative parameter sets. Thus, the degeneracy of the best fits was due to variations in the experimental data. The method of fitting was exhaustive, starting from more than 500 initial conditions and developing the parameter space for all possible best fits.

As an example, the lines in Fig. 1 show a typical best fit using $q = 2$, $\omega = 8$, $k_f = 1 \times 10^{-4}$ s^{-1}, $k_p = 2.5 \times 10^{-4}$ s^{-1}, and with $N_\omega(\text{GP4f}) = 680$ eight-mer aggregates and $N_\omega(\text{HAb2}) = 27{,}880$ eight-mer aggregates in the area of apposition. The root mean square error for this fit, over both data sets, was rmse $= 3.79 \times 10^{-2}$. For over 500 independent best fittings of the parameters, the minimum rmse $= 3.78 \times 10^{-2}$, using the fitting routine of MATLAB (fmins, The Math Works). Best fits were defined as having a rmse $\leq 3.9 \times 10^{-2}$. All the best fits were indistinguishable from the representative curve shown in Fig. 1.

The outcome of all these fittings is shown in Table 1:

1. The fits only weakly depended upon ω. Provided $\omega \geq 8$, any value of ω could be fitted and $\omega = 36$ was the largest attempted. Choosing $w \leq 7$ required values of $N_\omega(\text{HAb2}) > 7 \times 10^6/(3\omega)$, i.e., exceeding the maximal value of HAs available on the cell within the area of apposition.
2. Although the approximate solution could tolerate noninteger values of q, the numerical integration had to fix q at an integer value, and only $q = 2$ or 3 yielded best fits. For $q = 3$, the value of $k_p \geq 0.5$ s^{-1} was required, which made that step infinitely fast. Fig. 3 shows examples of optimized fits for $q = 1$ and $q = 4$, compared with a best fit for $q = 2$ from Fig. 1. A best fit for $q = 3$ is not shown because it is equivalent to that for $q = 2$. With $q = 1$, the optimized fits had rmse $\geq 6.1 \times 10^{-2}$ (minimum) and the fit is obviously poorer. With $q = 4$, the optimized fit

TABLE 1 Parameters of best fits (rmse $\leq 3.9 \times 10^{-2}$) for the nucleation model ($\omega = 8$ or 12) of HA aggregation*

q†	ω† (n = number of fits)	k_f (s^{-1})‡	k_p (s^{-1})‡	$\frac{N_\omega(\text{HAb2})}{N_\omega(\text{GP4f})}$§	N_ω(GP4f)¶ Nucleation Eqs. A6 and A7	$\approx N_\omega$(GP4f)‖ Eq. 11
2	8 ($n = 126$)	$(0.3–2) \times 10^{-4}$	$(0.3–7) \times 10^{-4}$	41 ± 2	416	$\approx 10^{-7.97\pm0.02}/(k_p k_f^{1.8})$
	12 ($n = 236$)	$(0.3–2) \times 10^{-4}$	$(0.3–5) \times 10^{-4}$	38 ± 3	898	$\approx 10^{-8.30\pm0.01}/(k_p k_f^{1.8})$
3	8 ($n = 38$)	$(0.4–2) \times 10^{-4}$	≥0.5	39 ± 3	416	$\approx 10^{-8.72\pm0.01}/(k_f^{2.8})$
	12 ($n = 38$)	$(0.3–1) \times 10^{-4}$	≥0.5	40 ± 2	898	$\approx 10^{-9.28\pm0.01}/(k_f^{2.8})$

*Best fit implies that the rmse (root mean square error) for all data points $\leq 3.9e-2$, where the minimum rmse $= 3.79 \times 10^{-2}$ for all fittings. All best fits are visually identical to the numerical integration shown on Fig. (1).

†Only $q = 2$ or 3 could best fit the data. Two different values of ω were fitted exhaustively and the total number of independent fittings that qualified as best fits are shown in parenthesis. For $q = 3$, the number of trials were smaller, $n = 38$, because the value for $k_p \geq 0.5$ needed only to be large enough to be infinitely fast. Thus, fewer trials adequately covered the parameter space.

‡Values of k_f and k_p: out of these ranges, either gave poor fits (rmse $\geq 3.9e-2$) or required more ωmer aggregates in the area of apposition than were available for these cells, see footnote ¶, below.

§Ratio of the number of ω-mers in the area of apposition for the two cell lines for all best fits from the numerical integrations (±SD).

¶The nucleation model predicts these values for the number of ωmers in the area of apposition for the GP4f cells, as derived from Eq. A6 and the results of Fig. 5. $N_\omega(\text{GP4f}) = (1 - f) \times 10^6/\omega$, because there are roughly 3×10^6 HAs/GP4f cell (Ellens et al., 1990) and roughly ⅓ of the cell surface is apposed to the planar bilayer, see Results and Fig. 1. γ was fitted to 3.4×10^{-3} for $\omega = 8$ and to 1.2×10^{-2} for $\omega = 12$, by the data in Fig. 5 for $N_\omega(\text{GP4f})/N_\omega(\text{HAb2}) = 40$. Using this value for N_ω(GP4f), with $q = 2$, $\omega = 8$, and $k_f = 1 \times 10^{-4}$ s^{-1}, gives a best fit with $k_p = 4.1 \times 10^{-4}$ s^{-1} by Eq. 11. This fit is visually identical to that shown in Fig. 1.

‖The fitted values of the N_ω(GP4f) from Eqs. 3 and 4 were estimated quite accurately by this formula, for values of k_f and k_p, within the ranges shown. This provides a parameter space of best fits, not all of which are physically meaningful, because the fits do not exclude values requiring more HA than is available. Because there are roughly 3×10^6 HAs per GP4f cell, N_ω(GP4f) must be less than $3 \times 10^6/(3\omega)$, because ⅓ of the HA aggregates will be in the area of apposition, and there are ω HA trimers per aggregate. This eliminates some possible fits. This upper bound is really too large, because it assumes all of the HAs form ωmers, which is not physically realistic. Because there are roughly 7×10^6 HAs per HAb2 cell, N_ω(HAb2) also must be less than $40 * (7/3) \times 10^6/\omega$, because there must be roughly 40 [$= N_\omega(\text{HAb2})/N_\omega(\text{GP4f})$] times more ωmers in the area of apposition for the HAb2 cells. This eliminates even more possible fits. The remaining set of values defines the parameter space of fits for the data of Melikyan et al. (1995), without the constraint of a reasonable HA binding model. The values given in the previous column for the nucleation model represent reasonable estimates for N_ω(GP4f) and a limitation for the parameter space of best fits (rmse $\leq 3.9e-2$). The exponent to 10 in the equation, e.g., 7.97 ± 0.02 for $q = 2$ and $\omega = 8$, shows the small effect of ω on the fits, because it only becomes 8.30 ± 0.01 for $\omega = 12$. The exponent to k_f appears to equal $q - 0.2$.

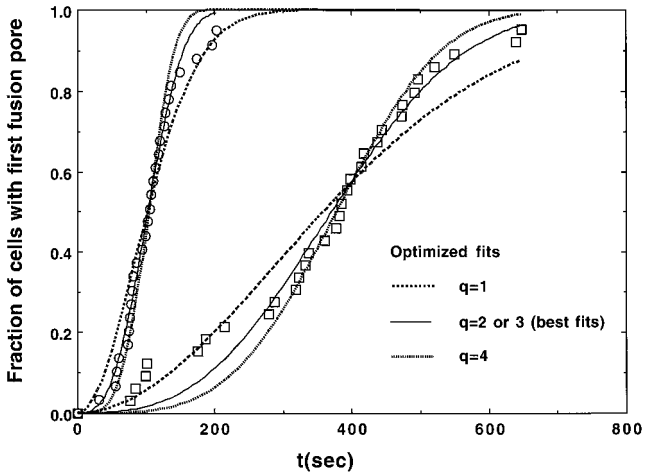

FIGURE 3 Optimized fits ($\omega = 8$) as a function of q show that numerically integrated, Eqs. 3 and 4, best fits require that $q = 2$ or 3. The data and $q = 2$ fit (*solid line*) are taken from Fig. 1. Best fits for $q = 3$ are visually identical to the fit in Fig. 1. For the $q = 1$ optimized fit (*heavy dashed lines*) the minimal rmse $\geq 6.5 \times 10^{-2}$, e.g., with $k_f = 1.0 \times 10^{-4}$ s^{-1}, $k_P = 3.7 \times 10^{-6}$ s^{-1}, and the number of fusogenic aggregates within the area of apposition for the GP4f cell line N_ω(GP4f) = 4000 and for the HAb2 cell line N_ω(HAb2) = 46,000 = 11.5 $*$ N_ω(GP4f), using Eq. 10. For the $q = 4$ optimized fit (*heavy dotted lines*) the minimal rmse $\geq 5.5 \times 10^{-2}$, e.g., with $k_f = 2.0 \times 10^{-4}$ s^{-1}, $k_f > 0.5$ s^{-1} (infinitely large) and the number of fusogenic aggregates within the area of apposition for the GP4f cell line N_ω(GP4f) = 445 and for the HAb2 cell line N_ω(HAb2) = 57,850 = 130 $*$ N_ω(GP4f), using Eq. 10. Obviously, the ratio of amplitude factors has changed radically from 40 also.

had rmse $\geq 5.5 \times 10^{-2}$ (minimum) and were visibly poorer than the $q = 2$ fit, e.g., compare the fits for the HAb2 data. The criteria of best fits having rmse $\leq 3.9 \times 10^{-2}$ provides a reliable means for estimating the values for the important parameters of these data.

3. The small range of acceptable values for $k_f \approx (0.3 - 2) \times 10^{-4}$ s^{-1} gives a very tight estimate for this rate constant of the essential HA conformational change. Basically, the same range was found using the approximate Eq. 8, proving its usefulness.
4. The fitted values for k_p fell into two ranges, depending upon whether $q = 2$ or 3. At present, it is only possible to state that k_p is either of the same order of magnitude as k_f (if $q = 2$) or it is at least 10^3 times faster (if $q = 3$). Analysis of other data will be required to determine which is the case.
5. For $\omega = 8$, the ratio of N_ω(HAb2)/N_ω(GP4f) = A(HAb2)/A(GP4f) = 40 $\pm$ 2, using Eq. 8 to calculate the amplitude factor, using only the $j = 0$ term for the nucleation model. Clearly, even the approximate solution estimates the ratio of the amplitude factors accurately, see Eq. 10, proving that this parameter is central to fitting the data.
6. The number of fusogenic aggregates within the area of apposition, N_ω(GP4f), according to the nucleation model, Eq. A.6 and Fig. 5 in the Appendix, are shown. This predicts that less than 1% of the HAs are in fusogenic aggregates, as discussed in Appendix A.
7. For the best fits, the fitted value of N_ω(GP4f) was uniquely fixed by k_f and k_p, according to the following empirically derived equation for the case of $\omega = 8$ and $q = 2$:

$$N_\omega(\text{GP4f}) = \frac{10^{-7.97 \pm 0.02}}{k_f^{1.8} k_p}. \quad (11)$$

The fit of this equation to the fitted values of N_ω(GP4f) was remarkably tight, suggesting a fundamental role for this equation in the model kinetics. This equation is similar to Eq. 10 for the approximate fits, because it shows that the number of fusogenic aggregates times the rate constants (to some power) is a constant. Parts of the parameter space defined by Eq. 11 are inaccessible because they would require N_ω(GP4f) and/or N_ω(HAb2) to exceed the available number of HAs in the area of apposition. For other values of ω and q, the coefficients are slightly different.

Because of the number of parameters involved, it is useful to show the sensitivity of the fits to variations in the parameters values. Figure 4 shows the curves generated by varying the parameter values, one at a time, from the fit of Fig. 1. In *Panel A*, q is changed from 2 to 1 or 3, i.e., a 50% variation, while the remaining parameters remain fixed: $k_f = 1 \times 10^{-4}$ s^{-1}, $k_p = 2.5 \times 10^{-4}$ s^{-1}, and N_ω(GP4f) = 680 ωmers in the area of apposition. N_ω(HAb2) is calculated as 41 $*$ N_ω(GP4f), which is the best fit value. The thick lines are the fits for the GP4f cell line, where $q = 1$ curve actually lies over the HAb2 data points whereas the $q = 3$ curve is much slower than the GP4f data. The thin lines are the fits for the HAb2 cell line, where $q = 1$ curve is much faster than the HAb2 data whereas the $q = 3$ curve actually lies nearer to the GP4f data points. Obviously, the fits are extremely sensitive to changing q, where the rmse = 0.514 for $q = 1$ and rmse = 0.498 for $q = 3$.

For the remaining parameters, the variation also will be fixed at $\pm$50% of the best fit values used in Fig. 1 to show the relative sensitivity of the fit to each parameter. In *Panel B*, k_f is changed by $\pm$50%, i.e., $\pm 0.5 \times 10^{-4}$ s^{-1}, to either 1.5×10^{-4} s^{-1} or 0.5×10^{-4} s^{-1}, while the remaining parameters remain fixed at the values used in Fig. 1. The thick lines are the fit for the GP4f cell line, where the larger value of k_f yields the curve that is faster than the GP4f data. The thin lines are the fit for the HAb2 cell line. Obviously, the fits are very sensitive to changing k_f, where the rmse = 0.205 for $k_f = 1.5 \times 10^{-4}$ s^{-1} and rmse = 0.312 for $k_f = 0.5 \times 10^{-4}$ s^{-1}.

In *Panel C*, k_p is changed by $\pm$50%, i.e., $\pm 1.25 \times 10^{-4}$ s^{-1}, to either 3.75×10^{-4} s^{-1} or 1.25×10^{-4} s^{-1}, while the remaining parameters remain fixed at the values used in Fig. 1. The thick lines are the fit for the GP4f cell line, where the larger value of k_p yields the curve that is faster

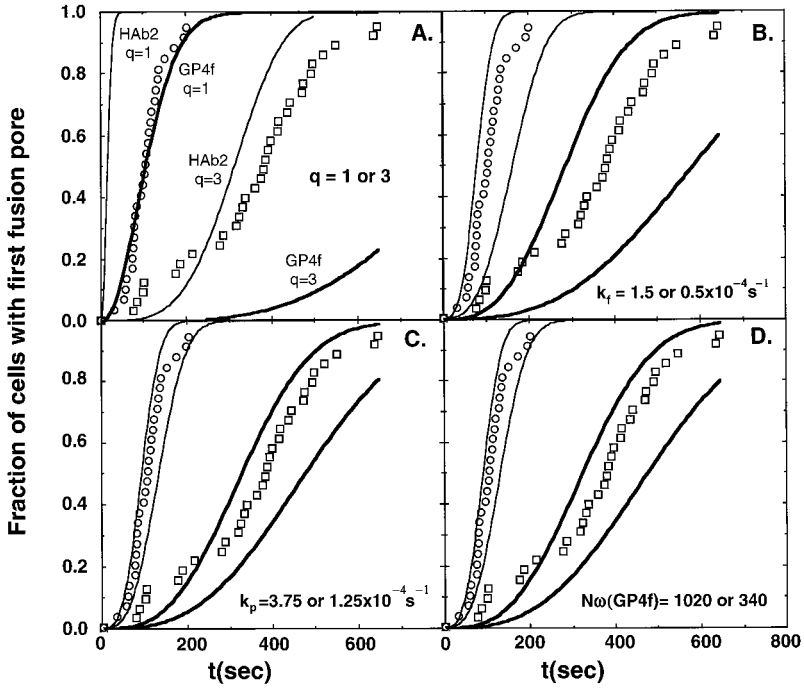

FIGURE 4 The sensitivity of the fits to the parameters is shown by altering the parameters from the best fit values used in Fig. 1. The thick lines are the fit for the GP4f cell line and the thin lines are the fit for the HAb2 cell line. (*A*) q is changed from 2 to 1 or 3, while the remaining parameters remain fixed. The thick lines are the fit for the GP4f cell line, where $q = 1$ curve actually lies over the HAb2 data points whereas the $q = 3$ curve is much slower than the GP4f data. The thin lines are the fit for the HAb2 cell line, where $q = 1$ curve is much faster than the HAb2 data whereas the $q = 3$ curve actually lies nearer to the GP4f data points. The rmse = 0.514 for $q = 1$ and rmse = 0.498 for $q = 3$. (*B*) k_f is changed by $\pm 0.5 \times 10^{-4}$ s^{-1} or 50%, to either 1.5×10^{-4} s^{-1} or 0.5×10^{-4} s^{-1}. The thick lines are the fit for the GP4f cell line, where the larger value of k_f yields the curve that is faster than the GP4f data. The thin lines are the fit for the HAb2 cell line. The rmse = 0.205 for $k_f = 1.5 \times 10^{-4}$ s^{-1} and rmse = 0.312 for $k_f = 0.5 \times 10^{-4}$ s^{-1}. (*C*) k_p is changed by 50% to match the variation of k_f in *Panel B*, so k_p is changed by $\pm 1.25 \times 10^{-4}$ s^{-1}, to either 3.75×10^{-4} s^{-1} or 1.25×10^{-4} s^{-1}, while the remaining parameters remain fixed at the values used in Fig. 1. The rmse = 0.114 for $k_p = 3.5 \times 10^{-4}$ s^{-1} and rmse = 0.180 for $k_p = 1.5 \times 10^{-4}$ s^{-1}. (*D*) N_ω(GP4f) is changed by 50% to match the variation of k_f in *Panel B*, so N_ω(GP4f) is changed by ± 340, to either 1020 8-mers or 340 8-mers. The rmse = 0.116 for N_ω(GP4f) = 1020 8-mers and rmse = 0.181 for N_ω(GP4f) = 340, i.e., nearly the same as for the variations in k_p.

than the GP4f data. The thin lines are the fit for the HAb2 cell line. The fits are sensitive to changing k_p, where the rmse = 0.114 for $k_p = 3.75 \times 10^{-4}$ s^{-1} and rmse = 0.180 for $k_p = 1.25 \times 10^{-4}$ s^{-1}.

In *Panel D*, N_ω(GP4f) is changed by $\pm 50\%$, i.e., ± 340, to either 1020 or 340 (8-mers), while the remaining parameters remain fixed at the values used in Fig. 1. The thick lines are the fit for the GP4f cell line, where the larger value of N_ω(GP4f) yields the curve that is faster than the GP4f data. The thin lines are the fit for the HAb2 cell line. The fits are as sensitive to changing N_ω(GP4f) as they are to changing k_p, because the rmse = 0.116 for N_ω(GP4f) = 1020 (8-mers) and rmse = 0.181 for N_ω(GP4f) = 340 (8-mers). This might be expected from the constraint equation of the best fit parameters shown in Eq. 11 and Table 1.

The effect of allowing a distribution of aggregate sizes was also examined. In particular, numerical integrations allowing for $[X_{\omega,q}(0)]$ to $[X_{\omega+10,q}(0)]$ to sustain fusion sites was studied in some detail. To introduce a minimum number of new parameters, a distributed aggregation model that had already been analyzed in Bentz and Nir (1981a,b) was used, where all possible aggregate sizes are allowed, see Appendix A. Remarkably, as explained in Appendix A, despite its seeming generality, the simplest version of this aggregation model could not provide good fits to the data. Basically, too many HAs were wasted in aggregates smaller than ωmers, as compared with the nucleation model. That is, to achieve a good fit, the ratio of the amplitude factors, A(HAb2)/A(GP4f) fitted by the data, as defined in Eqs. 8 or A.3, must be roughly 40. This requires that the HA-to-HA binding constant be relatively small, so that the 1.6-fold increase in HA surface density between the cell lines adequately increases the surface density of ωmers for the HAb2 line. The larger the value of ω, the larger the ratio of the ωmer surface densities. However, the larger the value of ω, the smaller the number of ωmers. For the simplest version of the distributed aggregation model shown in Appendix A, the absolute number of ωmers in the area of apposition fell below 10 before the ratio of the amplitude factors could exceed about 25, which yields poor fits to the data. The distributed aggregation model could yield adequate fits (using representative values for k_f, k_p, ω, and q found from the

nucleation model) if the HA surface density ratio were increased to 2 or above.

More importantly, best fits could be obtained for a ratio of HA surface densities of 1.6 using a hybrid nucleation/distribution model of aggregation, such that the binding constant increases with aggregate size (like nucleation) up to ω and then decreases with size (like distribution), as explained in Appendix A. Such a model is likely to match the thermodynamics of HA aggregation proposed by Kozlov and Chernomordik (1998). Nevertheless, an exhaustive analysis of these cases was not performed because extra parameters would have been needed, and no new information on the important fusion parameters appeared forthcoming, i.e., essentially the same parameter space fitted the data as shown in Table 1. In general, this result is fortuitous, because it will guide the elucidation of the proper aggregation model for HA, which appears to lay between the nucleation and this distributed model.

The primary deviation between the data and the fit was for the GP4f cells early on, where it appears that a fraction of the GP4f cells form the first fusion pore too rapidly. It is possible that a fraction of the GP4f cells (say 20%) are expressing higher HA surface densities. As mentioned, Ellens et al. (1990) measured the ratio of [HA(HAb2)]/[HA(GP4f)] = 1.9, from independent measurements of both cell surface densities. Danieli et al. (1996) only measured relative HA surface densities, and reported the relative densities as 1.6. Melikyan et al. (1995) did not measure the relative HA surface densities. So, it is possible that [HA(GP4f)] increased in the interim for some of the cells in the culture. These deviations are not important for the conclusions that we can reach, because the fits are quite good overall. Eliminating these early data points made no significant quantitative difference to the fitted parameters, although the slope of the fit at the midrange improved somewhat.

DISCUSSION

Low pH yields two or three major conformational changes in membrane-bound HA. The first change is the exposure of the N-terminus of HA2, the fusion peptide, which occurs rapidly compared to fusion and is required to promote fusion (Skehel et al., 1982; White and Wilson, 1987; Ruigrok et al., 1988; Stegmann et al., 1990; Godley et al., 1992; Stegmann and Helenius, 1993; Pak et al., 1994). The second conformational change is the formation of the extended coiled coil of HA2, which was predicted by Carr and Kim (1993), proven for a fragment of HA (TBHA2, residues 38–175 of HA2 and 1–27 of HA1 held together by the disulfide bond) by crystallography (Bullough et al., 1994; Chen et al., 1995), morphologically observed for HA on intact virus using cryoelectron microscopy (Shangguan et al., 1998), and suggested on HA-expressing cells using site-directed mutagenesis (Qiao et al., 1998). The formation of the extended coiled coil would relocate the N-terminus of HA2 approximately 100 Å toward the target membrane. A third change was observed in the crystal structure of TBHA2 fragment (Bullough et al., 1994), wherein the C-terminus of the original coiled coil had flipped up in a helix-turn transition, creating an antiparallel α-helical annulus at the base of the extended coiled coil. It is not known that this conformational change can occur with membrane-bound HA (Shangguan et al., 1998).

The essential problem in HA-mediated fusion is to correlate these individual conformational changes of HA with the communal intermediates of the fusion process. The kinetic model and analysis presented here clearly demonstrate that the formation of the first fusion pore, which is the earliest measurable event in the fusion process, requires an aggregate of HAs. The minimal HA aggregate size (ω) capable of sustaining fusion was at least 8, and may well be much larger. However, only $q = 2$ or 3 of those HAs within the ωmer aggregate needed to undergo the essential conformational change slowly for the first fusion pore to form.

The fits (approximate and numerically integrated) were very sensitive to the value of minimal fusion unit q, as shown by Figs. 3 and 4. If the data had required $q = 0$, for a concerted process, as used theoretically in Bentz (1992) and proposed by Kozlov and Chernomordik (1998), or $q = \omega$, for a wholly independent and identical process, as prescribed by Blumenthal et al. (1996), then the fitting of these data would have demanded it. That $q = 2$ or 3, introduces a concept both novel and constraining for any molecular model of HA-mediated fusion.

The other important fitted parameter is k_f, the rate constant for the essential conformational change. It is widely believed that the formation of the extended coiled coil is essential for HA-mediated fusion (Skehel and Wiley, 1998). Normally, the rate of formation of a coiled coil would be roughly 10^3 s^{-1}, depending upon initial conditions (Brandon and Tooze, 1991; Sosnick et al., 1996). The rate of the essential conformational change measured here, $k_f \approx 10^{-4}$ s^{-1}, is roughly 7 orders of magnitude slower. Thus, although the formation of the extended coiled coil might be the essential conformational change for the first fusion pore, something must be slowing it down substantially.

Before discussing why the essential conformational is so slow, we must first answer the question: How can fusion happen in 100–200 s (Fig. 1) if the essential conformational change for HA occurs only in 10^4 s on average? This is very important. First, the conformational change of the protein must follow a probabilistic distribution over time, which is expected, so that a few transform within seconds to minutes and more transform as time passes. Obviously, this speaks only to the waiting time for the conformational change, because the change itself should require much less time. Second, Melikyan et al. (1995) only monitor the very first of roughly hundreds (on the GP4f cell line) or thousands (on the HAb2 cell line) fusogenic HA aggregates, (see Results

and Appendix A), which succeed in forming the first fusion pore. The essence of fusion is to look at the first of the ensemble to succeed in having 2 or 3 HAs transform under the right circumstances, i.e., the winner of the race. The average of the ensemble is much slower than the first passage time.

Any proposed model for HA-mediated fusion must have a mechanistic role for q and some reason that the essential conformational change is so slow. A role for at least 8 HAs as the minimal aggregate size would also be desirable. We will find that none of the current published models for fusion completely comply with all of these constraints. In fact, Epand et al. (1999) have claimed that a fragment of HA with a preformed extended coiled coil can cause liposome–liposome lipid mixing with a particular composition of lipids. It remains to be shown that their system follows the same path for bilayer destabilization as full-length HA in a membrane.

Correlating individual conformational changes of HA with the communal intermediates of the fusion process is difficult because of our lack of kinetic knowledge. It is not known how long transformation to the extended coiled coil requires for bromelain-solubilized hemagglutinin. For the native system, i.e., virions, Shangguan et al. (1998) found that the formation of the extended coiled coil on isolated PR-8 virions, visualized by cryoelectron microscopy, occurred on a time scale far slower ($>$2000 s) than that of fusion ($<$400 s) for the virions with ganglioside-bearing liposomes. At first glance, such a result appeared to relegate the formation of the extended coiled coil to HA to inactivation rather than fusion. However, we preferred the idea that the energy released by the coiled coil formation was directly coupled to the destabilization of the apposed membranes (Shangguan et al., 1998). The problem of the discrepant time scales might have been resolved if the close approach of the target membrane or the binding of HAs to receptors accelerated the formation of the extended coiled coil. However, prior work suggested to the contrary that the HAs that mediate fusion are not the ones bound to the sialoside receptors on the target membrane, and that binding to the sialoside receptors would slow down the conformational change in any case (Ellens et al., 1990; Alford et al., 1994). Thus, no mechanism for acceleration of the conformational change was available.

Now we find that the time constant for the essential conformational change leading to the first fusion pore is roughly the same as that found for the formation of the extended coiled coil on the isolated PR8 virions, i.e., 10^3–10^4 s. The cell lines analyzed here express the Japan strain of HA, which has slower and less complete inactivation kinetics than PR8 (Puri et al., 1990; Körte et al., 1997, 1999). Thus, the similarity of time scales is striking. Evidently, cryoelectron morphological results can determine when the majority of the HAs form the extended coiled coil. It strongly suggests that the same conformational change can create both the slow average kinetics of extended coiled coil morphology visualized in Shangguan et al. (1998) and the relatively rapid formation of the first fusion pore.

Now we can consider why the essential conformational change might be so slow. Several slow steps for fusion have been proposed, the most common being rearrangements of HAs after extended coiled coils form and fusion peptides are embedded in the target membrane, including a helix–coil transition at the base of the HA2 extended coiled coil in some cases (Bullough et al., 1994; Yu et al., 1994; Chen et al., 1995; Hernandez et al., 1996; Blumenthal et al., 1996; Zimmerberg et al., 1994; Carr et al., 1997; Chernomordik et al., 1997, 1998; Durell et al., 1997; Qiao et al., 1998). All of these models fall into the category of having fusion rate limited by aggregation of activated HAs, which was shown in Appendix B as not being able to fit the data of Melikyan et al. (1995) in any simple way. Thus, it seems likely that the rate-limiting step is simply the slow formation of the extended coiled coil for the HAs on the fusion pathway. This agrees with the suggestion of Plonsky et al. (1999) that the fusion induced by the baculovirus protein GP64 is not rate limited by the aggregation of GP64 (Markovic et al., 1998) into a pore.

After the N-terminus of HA2 is released by low pH and before it can reach the target membrane, it can reside in either of two places: in the aqueous space between the apposed membranes or embedded in the viral envelope/HA-expressing cell membrane (Bentz et al., 1990; Gaudin et al., 1995; Kozlov and Chernomordik, 1998). These two positions should yield very different times for transforming to the extended coiled coil, and it is not known which is on the fusion pathway, because the HAs probably refold through several pathways within the folding landscape.

If the fusion pathway began with the fusion peptide suspended in the aqueous space between the two membranes, then the most straightforward mechanism for inhibiting the formation of the extended coiled coil is a slow separation of the HA1 headgroups, which is required for the conformational change to the extended coiled coil (Bullough et al., 1994; Carr et al., 1997; Shangguan et al., 1998). This dissociation has been postulated to be involved in HA-mediated fusion (Gray and Tamm, 1997, 1998), although there is no evidence that HA1 is involved in the initial destabilization. The timer that determines when dissociation occurs is unknown. There are no significant hydrophobic or ion-pair groups holding the HA1 headgroups together and, once dissociated, they freely move through the rotation of a single bond and cannot reassociate due to steric hindrance from the extended coiled coil (Shangguan et al., 1998). However, White and Wilson (1987) found that the epitope exposure of X-31 BHA corresponding to dissociation of the HA1 headgroups occurred within 10 min at 37°C. Even with the kinetic differences between the X-31 and Japan strain, these results strongly suggest that headgroup dissociation is not the essential conformational change.

Furthermore, to postulate that slow dissociation of the HA1 headgroups is the essential conformational change for

fusion does not clarify the meaning of $q = 2$ or 3, nor does it actually suggest a fusion mechanism. Simply having the fusion peptides from 2 or 3 trimers reach the target membrane after spending a long time suspended between the membranes does not give any function for the substantial free energy released upon formation of the extended coiled coil (Dieckmann et al., 1998; Kozlov and Chernomordik, 1998). Once the fusion peptide reaches the target membrane, all of that energy will be dissipated. There are no batteries evident in this system. Nor is it clear how the slow dissociation of $q = 2$ or 3 headgroups could either make fusion happen alone or alter the structure of the other neighboring HAs to lead to a cooperative conformational change. Knowing how long it takes BHA to transform to the extended coiled coil will be necessary to reach a conclusion.

The proposal that the helix-turn transition near the transmembrane domain brings the apposed membranes together through a bending of the membranes (Bullough et al., 1994; Hernandez et al., 1996; Weissenhorn et al., 1997, 1998; Qiao et al., 1998) overlooks the difficulty of bending membranes. This transition could donate much less free energy to the initial membrane defect than could the formation of the extended coiled coil, because it is essentially the exchange of one set of hydrophobic interactions for another equivalent set. Bending membranes has been calculated to require the concerted efforts of all or most of the HAs in the aggregate of six or more HAs to form the extended coiled coil (Kozlov and Chernomordik, 1998). It is difficult to imagine how the helix-turn transition from 2 or 3 trimers could create the bending energy required to qualify as the essential conformational change, even if it occurs on the virus or HA-expressing cell.

Having the fusion peptide of HA embedded in the viral envelope, which either frustrates (Kozlov and Chernomordik, 1998) or inhibits (Bentz, 1999) the formation of the extended coiled coil, would obviously slow down the essential conformational change substantially. Ruigrok et al. (1988) originally suggested that embedding the fusion peptide into the viral envelope could represent a step in fusion, but photolabeling work led to the belief that this configuration represented inactive HA (Brunner and Tsurudore, 1993; Wharton et al., 1995; Qiao et al., 1998). However, Kozlov and Chernomordik (1998) have resurrected this idea and proposed a fusion model that begins with the HA fusion peptides embedded into the viral envelope. In this configuration, the formation of the extended coiled coil is frustrated because the embedded fusion peptide requires substantial free energy or tension to be removed. This causes a deformation of the viral/HA-expressing cell membrane. The free energy cost of this deformation per HA is reduced by having HAs aggregate. This is a very elegant mechanism for producing HA aggregation.

The initial bilayer destabilization leading to fusion must involve hydrophobic defects and/or high curvature. The model of Kozlov and Chernomordik (1998) invokes the high bilayer curvature mechanism and it agrees with some of the data analyzed here, including the need for a large minimal aggregation unit. However, following aggregation, their mechanism for the formation of the first fusion pore requires that most or all of the HAs at the nascent fusion site bend away from the center of the fusion site to create a lipidic stalk rising from the viral envelope. This is a simultaneous or concerted event, i.e., with a $q = 0$, which does not fit the data described here. It could be argued that the remaining HAs at the fusion site quickly and cooperatively bend, but such cooperativity among the HAs is difficult to explain and, because such a step would not be rate limiting to fusion, even more difficult to prove.

Thus, the kinetic analysis does not support their model as being the rate-limiting step of the initial membrane destabilization. In contrast, it is likely that the curvature-based intermediates they and others have proposed occur later in the sequence of fusion intermediates (Chernomordik et al., 1998, 1999; Raznikov et al., 1998). That is, the initial high energy destabilization, for which $q = 2$ or 3, is followed by a sequence of intermediates leading to the various measurable steps of fusion. Interestingly, Shangguan et al. (1996) found that HA-mediated fusion was both very leaky and insensitive to target membrane material properties under optimal fusion conditions. Later, Chernomordik et al. (1997) found that fusion became sensitive to membrane material properties using suboptimal conditions, such as higher pH and lower temperatures. That is, the membrane material properties become kinetically significant as suboptimal conditions inhibit HA's fusogenic capacity.

In fact, the kinetic analysis shown here provides a new twist to this question of whether the photolabeling studies of HA on virions actually distinguish which fusion peptides are on the fusion pathway and which are not (Bentz et al., 1990; Stegmann et al., 1990; Durell et al., 1997; Qiao et al., 1998). Photolabeling studies typically find that a fraction ($\leq$10%) of the N-termini of HA2 are labeled from the target membrane after low pH treatment and before the onset of lipid mixing between the membranes (Brunner and Tsurudome Brunner, 1993; Stegmann and Helenius, 1993; Gaudin et al., 1995; Durell et al., 1997; Qiao et al., 1998). These results are consistent with the claim that fusion is initiated by those fusion peptides that were inserted into the target membrane, because they were there before fusion started. However, do the photolabeling studies prove that claim? A crucial experiment still missing is a comparison of the kinetics of fusion with the fraction of fusion peptides embedded in the target membrane before fusion as a function of HA surface density.

Melikyan et al. (1995) only monitor those HA aggregates that contribute directly to fusion, and k_f reflects only their rate of passage. HAs whose HA2 N-termini transformed directly from the aqueous space between the bilayers to the extended coiled coil should reach the target membrane much sooner than those embedded in the viral envelope, and

thus be photolabeled before fusion began. As estimated in Table 1, more than 90 to 99% of the HAs on the cell surface are not even in fusogenic aggregates, even though they would certainly undergo the essential conformational change. Perhaps HAs whose fusion peptides reside in the aqueous space between the apposed membranes transform rapidly to the extended coiled coil and embed their fusion peptides into the target membrane. Without any significant change to the quantitative conclusions of this work, more than 10% of the HAs on the cell surface could be allocated to follow any particular nonfusogenic pathway. This could explain the photolabeling data to date without yielding any conclusion about which fusion peptides are on the fusion pathway. By the models proposed in Kozlov and Chernomordik (1998) and in Bentz (2000), the photolabeling would be of HAs not involved in the initial destabilization of the membranes. The HAs refolding on the fusion pathway would have their fusion peptides initially embedded into the viral envelope. It is possible that the fusion pathway requires that the fusion peptides start in the viral envelope and end up in the target membrane to fulfill entirely different functions at each site.

The kinetic model described here quantifies the essential kinetic parameters of the first step of the HA fusion mechanism. There is a large minimal aggregation size, $\omega \geq 8$, and, within the aggregate, a small minimal fusion unit, $q = 2$ or 3. Any molecular model for HA-mediated fusion needs to explain this result. The finding that the rate constant of the essential conformational change for the formation of the first fusion pore is at least two orders of magnitude slower than the measured event is a clear illustration that fusion is due to the first intermediate that succeeds. From the more detailed analysis of HA surface aggregation given in Appendix A, it is clear that, although 8 is the lower bound for HAs at the fusion site, knowledge of the mechanism of HA aggregation will be needed to rigorously fix this number. The model of Kozlov and Chernomordik (1998) provides a good starting point for this calculation. Finally, these data are much more easily explained by a model of rapid HA aggregation following low pH exposure of its fusion peptide, where the fusion is rate limited by the slow conformational changes of HA. The model of fusion rate limited by aggregation of activated HAs simply does not readily fit the data.

The results in this work are consistent with the molecular model for HA-mediated fusion proposed in Bentz (2000). In this model, the committed step for fusion occurs when the extended coiled-coil transition occurs for those HAs in an aggregate so closely packed that the flow of outer monolayer viral lipids into the fusion site is restricted. This state of restricted lipid flow has been experimentally observed repeatedly (Tse et al., 1993; Zimmerberg et al., 1994; Blumenthal et al., 1996; Chernomordik et al., 1997, 1998), but never suggested as an essential step of fusion. Interestingly, close packing seems to be the end product of the aggregation model of Kozlov and Chernomordik (1998). The removal of the hydrophobic sidechains of $q = 2$ or 3 fusion peptides from the center of the site of restricted lipid flow would expose a patch of acyl chains from the viral outer monolayer to water. Thus, the formation of the extended coiled coil would create a high-energy transition state. Moreover, the closely packed HAs are inhibited from diffusing away from the site to admit lateral lipid flow to fill the defect, partially because that would increase the area of hydrophobic exposure to water. Thus, the other HAs in the aggregate stabilize this high-energy transition state, giving an important role for the minimal aggregate size. Destabilization of the apposed target membrane is one means of recruiting lipids to cover the exposed acyl chains on the viral outer monolayer, thus causing the initial joining of the membranes, probably by a lipidic stalk. Subsequent steps of fusion would depend upon membrane curvature effects, such as those reviewed in Chernomordik et al. (1999).

APPENDIX A. EQUILIBRIUM AGGREGATION MODELS FOR HA

The surface aggregation of HA trimers induced by low pH can be modeled as a mass action process (Bentz and Nir, 1981a,b; Bentz et al., 1988):

$$X_i + X_j \underset{r_{ij}}{\overset{a_{ij}}{\rightleftharpoons}} X_{i+j}, \tag{A1}$$

and so on to higher orders of aggregation. X_i denotes a surface aggregate of i HA trimers, a_{ij} and r_{ij}, denote the association and dissociation rate constants.

For aggregation on a surface, the diffusion rate-limited mass-action kinetics are not as simple as in a three-dimensional solution (Torney and McConnell, 1983; Molski et al., 1996). However, because the lateral diffusion coefficient for HA in the cell membrane is rapid, $D \approx 10^{-9}$ cm^2/s (Ellens et al., 1990), it is possible to show that the equilibrium distribution for HA aggregation should be achieved well before fusion occurs. If at least 10% of the HA–HA collisions are productive for aggregation, then the value of a_{11} is bounded by $2D \geq a_{11} \geq 2D/10 \approx 2 \times 10^{-10}$ cm^2/s (Torney and McConnell, 1983). The initial surface density of HAs on the GP4f cells is $[X_0] \approx (3 \times 10^6$ HA/cell)/(1800 μm^2/cell) $= 2 \times 10^{11}$ HA/cm^2 (Ellens et al., 1990). For general aggregation processes, Bentz and Nir (1981a,b) found that equilibrium was effectively reached after times $>10/a_{11}[X_0]$. Thus, after times $>10/[(2 \times 10^{-10}) \times (2 \times 10^{11})]$ s $= 0.25$ s, HA aggregation equilibrium will be established. This is well before first fusion pores form. It is interesting to note that the same equilibration time in a three-dimensional solution of the same volume (assuming the cell is a sphere) is less than 10^{-4} s. Appendix B pursues this question from a different angle, showing that the simplest HA aggregation rate-limited fusion model really cannot fit the data of Melikyan et al. (1995).

Let $[X_0]$ denote the initial surface concentration of HA trimers at neutral pH. After low pH treatment, HA aggregation is rapid and reversible as discussed above, and the equilibrium surface density of HA aggregates is given by

$$[\bar{X}_j] = \mathrm{E}(j)[\bar{X}_1]^j, \quad \mathrm{E}(1) \equiv 1, \quad \mathrm{E}(j) = \prod_{i=1}^{j-1}(a_{1i}/r_{1i}),$$

$$[X_0] = \sum_{j=1}^{\infty} j[\bar{X}_j] = \sum_{j=1}^{\infty} j\mathrm{E}(j)[\bar{X}_1]^j, \tag{A2}$$

where $[X_j]$ is the equilibrium surface density of j-mer aggregates, and the final equation gives the conservation of HA trimers, which is accurate provided not many trimers are consumed by the fusion intermediates, which is reasonable because only the first fusion pore is being monitored. Thus, to solve for the equilibrium distribution, we need to know the values of the E(j).

We can calculate expected values for the amplitude factors A(GP4f) and A(HAb2), using Eq. 8 and replacing $[X_{\omega,0}\ (0)]$ by the equilibrium distribution value $[X_\omega]$,

$$\frac{A(\mathrm{HAb2})}{A(\mathrm{GP4f})} = \frac{\delta(\mathrm{HAb2})\sum_{j=0}\frac{(\omega+j)!}{(\omega+j-q)!\,q!}[\bar{X}_{\omega+j}(\mathrm{HAb2})]}{\delta(\mathrm{GP4f})\sum_{j=0}\frac{(\omega+j)!}{(\omega+j-q)!\,q!}[\bar{X}_{\omega+j}(\mathrm{GP4f})]}. \quad \text{(A3)}$$

In particular, the ratio of the fusion-competent aggregates for two cell lines can be estimated from the ratio of the amplitude factors for the two cell lines. We know that the initial HA surface densities $[X_0(\mathrm{HAb2})]/[X_0(\mathrm{GP4f})] = 1.6–1.9$ (Ellens et al., 1990; Danieli et al., 1996). The ratio of $\delta(\mathrm{HAb2})/\delta(\mathrm{GP4f}) \sim 1.4$, because the HAb2 cells were roughly 40% larger than the GP4f cells (Ellens et al., 1990), and we assume that the cells have the same morphology against the planar bilayer. So, to find ω, we need to choose a value for $\alpha[X_0(\mathrm{GP4f})]$, which fixes $\alpha[X_0(\mathrm{HAb2})] = (1.6–1.9) * \alpha[X_0(\mathrm{GP4f})]$, and then find the value of ω such that Eq. A3 equals 40, per the fits summarized in Table 1.

Obviously, to do this calculation, a particular aggregation model must be chosen, and it is not known how HA aggregates. Nevertheless, we will examine two models chosen to give extreme conditions. We will consider a nucleation model, chosen to provide the smallest possible value for the minimal aggregate size ω, and we will consider a very simple distributed model to show why the minimal aggregate size ω is likely to be somewhat larger than that predicted by the nucleation model.

Nucleation: The minimal aggregation model

The nucleation aggregation reaction is

$$\omega X_1 \overset{K}{\rightleftharpoons} X_\omega, \quad \text{(A4)}$$

where $K = [X_\omega]/[X_1]^\omega$ is the equilibrium constant, which can be related to the formalism given in Eq. A2, but that is not essential here.

This model allows no aggregates smaller than those capable of sustaining fusion, which does not waste HAs in unfusogenic aggregates. It also allows no aggregates larger than ωmers, which, although (presumably) fusogenic, would also waste HAs. Therefore, it will predict the smallest value of ω for the minimal fusogenic aggregate size compared with other, likely more reasonable, aggregation models. The fraction of HAs in monomeric form is fixed by

$$[X_0] = [\bar{X}_1] + \omega[\bar{X}_\omega] = [\bar{X}_1] + \omega K[\bar{X}_1]^\omega. \quad \text{(A5)}$$

When $f = [\bar{X}_1]/[X_0]$ denotes the fraction of monomers at equilibrium, Eq. A5 can be divided by $[X_0]$ to yield

$$1 = f + \gamma f^\omega, \quad \text{where} \quad \gamma \equiv \omega K[X_0]^{\omega-1}. \quad \text{(A6)}$$

f can be solved as a function of γ and ω. The maximal change in the number of fusogenic aggregates due to a change in HA surface density occurs when γ is near 0 and $f \approx 1 - 1/(\omega + 1/\gamma)$. This is the domain needed to achieve large values for the ratio of the amplitude factors, Eq. A3.

For a given γ, the values of f(GP4f) and f(HAb2) can be calculated from Eq. A6, because $\gamma(\mathrm{HAb2}) = \gamma(\mathrm{GP4f})\varepsilon^{\omega-1} = \gamma\varepsilon^{\omega-1}$, when we denote the ratio of initial HA cell surface densities as $\varepsilon = [\mathrm{HAb2}]/[\mathrm{GP4f}]$. The ratio of amplitude factors can be written from Eq. A3 as

$$\begin{aligned}\frac{A(\mathrm{HAb2})}{A(\mathrm{GP4f})} &= \frac{\delta(\mathrm{HAb2})[\bar{X}_\omega(\mathrm{HAb2})]}{\delta(\mathrm{GP4f})[\bar{X}_\omega(\mathrm{GP4f})]} \\ &= \left(\frac{\delta(\mathrm{HAb2})}{\delta(\mathrm{GP4f})}\right)\left(\frac{[\mathrm{HAb2}](1-f(\mathrm{HAb2}))/\omega}{[\mathrm{GP4f}](1-f(\mathrm{GP4f}))/\omega}\right) \\ &= \left(\frac{\delta(\mathrm{HAb2})}{\delta(\mathrm{GP4f})}\right)\left(\varepsilon\,\frac{\gamma\varepsilon^{\omega-1}f(\mathrm{HAb2})^\omega}{\gamma f(\mathrm{GP4f})^\omega}\right) \\ &= \left(\frac{\delta(\mathrm{HAb2})}{\delta(\mathrm{GP4f})}\right)\left(\varepsilon\,\frac{f(\mathrm{HAb2})}{f(\mathrm{GP4f})}\right)^\omega \\ &< \left(\frac{\delta(\mathrm{HAb2})}{\delta(\mathrm{GP4f})}\right)\varepsilon^\omega. \end{aligned} \quad \text{(A7)}$$

The inequality follows because f decreases with increasing HA surface density. The graph of the predicted value of ω as a function of the ratio of the fitted value of A(HAb2])/A(GP4f) is shown in Fig. 5. Clearly, because A(HAb2])/A(GP4f) = 40, $\omega > 7$. Below, it is shown that more reasonable aggregation models would predict a larger minimal fusogenic aggregate size.

If $\gamma = 0.001$, then the number of fusogenic aggregates in the area of apposition (⅓ of the cell) is calculated to be $N_\omega = 135$ for the GP4f cell line, or 0.03% of the available 3×10^6 HAs on the cell, and there would be roughly $N_\omega = 5200$ aggregates for the HAb2 cell line, or 0.6% of the available 7×10^6 HAs. If $\gamma = 0.01$, then $\omega \sim 11$, and the number of fusogenic aggregates in the area of apposition (⅓ of the cell) is calculated to be roughly $N_\omega = 800$ for the GP4f cell line, or 0.3% of the available 3×10^6 HAs on the cell, and there would be roughly $N_\omega = 32{,}000$ aggregates for the HAb2 cell line, or 5% of the available 7×10^6 HAs.

Thus, the first fusion pore forms when the first of roughly hundreds (GP4f) or thousands (HAb2) of fusogenic aggregate sites succeeds. This explains why the average time for the essential conformational change (roughly 10^4 s) can be two orders of magnitude slower than fusion.

A distributed aggregation model

The nucleation model is quite restrictive and is unlikely to accurately depict the HA aggregation process, as might be predicted from the model of Kozlov and Chernomordik (1998), for example. Other aggregates are likely to form, and their behavior may be very important for understanding the overall fusion process. For example, Chernomordik et al. (1998) find, at low HA surface densities, that only hemifusion is observed. Perhaps aggregates smaller than ωmers can cause some membrane destabilization, without sustaining fusion. The nucleation model could not predict this, because there are only HAs and ωmers. A distributed model, allowing all possible j-mers to coexist at equilibrium is more realistic. In Bentz and Nir (1981a,b), we examined one classification scheme for the higher order equilibrium constants, such that

$$\frac{a_{1i}}{r_{1i}} = \alpha\left(\frac{2}{1+i}\right)^\beta, \quad \text{(A8)}$$

where $\alpha = (a_{11}/r_{11})$ and β is just a parameter that permits a simple functional dependence for the (unknown) many body effects in the higher order aggregates. This scheme is one way to describe the general behavior

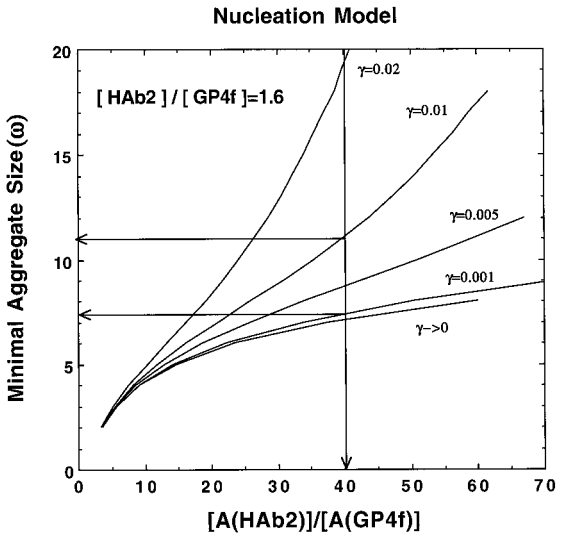

FIGURE 5 The value of ω as a function of possible A(HAb2)/A(GP4f) values assuming a nucleation model, where only aggregation to ωmers is allowed, calculated by Eqs. A4–A7. The ratio of the HA surface densities was 1.6, δ(HAb2)/δ(GP4f) = 1.4 (Ellens et al., 1990) and γ is defined for the GP4f cell line. The arrow at A(HAb2)/A(GP4f) = 40 shows which value is required by the fit in Fig. 1. In the limit of vanishingly small HA surface densities, i.e., the extreme case of $\gamma \rightarrow 0$, the vertical arrow shows that the minimal aggregate size is just under 8 HAs. This is the lowest bound for ω, because larger HA surface densities or any other aggregation model, see Figs. 5 and 6, would predict a larger value for ω. For the case of $\gamma = 0.001$, the calculation predicts roughly N_ω(GP4f) = 120 8-mer aggregates in the area of apposition for the GPf4 cells out of the roughly 3×10^6 HAs on the cell (or 0.03% of the total HAs) and roughly N_ω(HAb2) = 4800 8-mer aggregates in the area of apposition for the HAb2 cells out of the roughly 7×10^6 HAs on the cell (or 0.5% of the total HAs). Uncertainties in the relative areas of apposition, i.e., whether δ is ⅓ or ½ of the cell surface area are not very significant.

of aggregation equilibrium when the specific interactions between the particles are unknown. We can use it here to examine the effort of a distribution of HA aggregates on the expected fusion kinetics and compare the predictions with those of the nucleation model.

When $\beta = 0$, so that all equilibrium constants are equal, using Eq. A8 in A2 yields

$$E(j) = \alpha^{j-1}$$

$$\alpha[X_0] = \alpha \sum_{j=1}^{\infty} j(\alpha)^{j-1}[\bar{X}_1]^j = \frac{\alpha[\bar{X}_1]}{(1 - \alpha[\bar{X}_1])^2}$$

$$\Rightarrow \alpha[\bar{X}_1] = \frac{2\alpha[X_0] + 1 - \sqrt{4\alpha[X_0] + 1}}{2\alpha[X_0]}. \quad \text{(A9)}$$

So, the value of $\alpha[X_1] < 1$ is easily solved for a given value of $\alpha[X_0]$. When $\beta = 1$, we obtain

$$E(j) = (2\alpha)^{j-1}/j! \quad \text{(A10)}$$

$$\alpha[X_0] = \alpha \sum_{j=1}^{\infty} j(2\alpha)^{j-1}[\bar{X}_1]^j/j!$$

$$= \alpha[\bar{X}_1]\exp\{2\alpha[\bar{X}_1]\}.$$

Although this equation is not analytically invertible, the value of $\alpha[X_1]$ is easily solved numerically for a given value of $\alpha[X_0]$.

As it turns out, if the ratio of HA surface densities is only 1.6 and $\beta = 0$ (or even worse, $\beta = 1$), the ratio of amplitude factors A(HAb2)/A(GP4f) cannot exceed ~25 before there are fewer than 10 fusogenic aggregates, which yields poor fits to the data. This aggregation model wastes too many HAs in unproductive aggregates, i.e., those that are too small to sustain fusion. Simply increasing both surface densities of HA does not solve the problem, because it is the ratio of HA surface densities that is too small.

This is an unexpected and fortuitous result, because it gives an analytical standard to start testing more realistic aggregation models. For example, it was possible to achieve best fits to the data (rmse $\leq 3.9e-2$), i.e., visually identical to the nucleation fits shown in Fig. 1 by assuming, for Eq. A8, that $\beta = -1$ for $j \leq \omega$ and $\beta = 0$ or $+1$ for $j > \omega$, using $\omega \geq 8$. This is a hybrid model between nucleation, because it has increasing affinity for the binding until the critical size ω is reached, and distribution, because it has decreasing affinity for the binding after the critical size ω is reached. This type of model is likely to fit the thermodynamics proposed by Kozlov and Chernomordik (1998). A sampling of fittings using this model did not appear to show any fundamental differences from the fits to the nucleation model. Because this aggregation model does require choosing values for α and ω, and the break at $j = \omega$ is arbitrary, it seems there is no need to pursue this analysis further here.

For the sake of understanding the behavior of a distribution-type model without introducing more parameters, we will use the ratio of HA surface densities [HAb2]/[GP4f] = 1.9, as it was estimated in Ellens et al. (1990). Figure 6 shows the calculations for the value of ω as a function of possible A(HAb2)/A(GP4f) values for the case of $\beta = 0$, using Eq. A3, for several

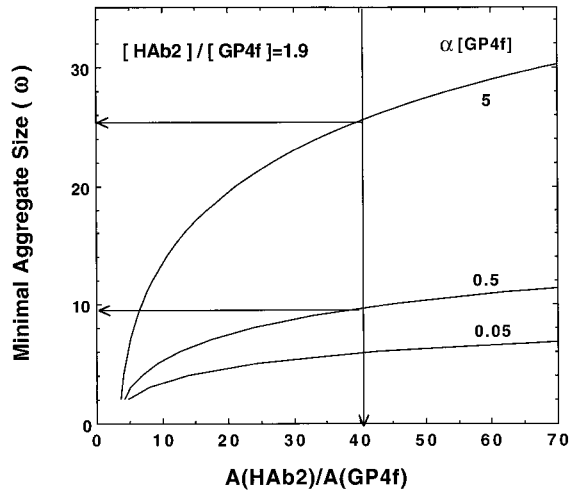

FIGURE 6 The value of ω as a function of possible A(HAb2)/A(GP4f) values assuming a distribution model of $\beta = 0$ and several values for $\alpha[X_0] = \alpha$[GP4f], calculated using by Eas. A4, A6, and A7. The ratio of the initial HA surface densities was [HAb2]/[GP4f] = 1.9, because a ratio of 1.6 would not fit the fusion data, as explained in the text. The arrow at A(HAb2)/A(GP4f) = 40 shows which value is required by the data of Melikyan et al. (1995) fitted in Fig. 1, as done in Fig. 5. For the case of $\alpha[X_0$(GP4f)] = 0.5, the vertical arrow shows that the minimal aggregate size is 6 HAs, but this case would have fewer than one fusogenic aggregate. The text describes the analysis that suggests that $\alpha[X_0$(GP4f)] > 0.5, so that the number of fusogenic aggregates is about 10, so that the minimal aggregate size $\omega \geq 10$. For the case of $\alpha[X_0$(GP4f)] = 5, the vertical arrow shows that the minimal aggregate size is about 26 HAs, and this case also has about 7 fusogenic aggregates. Other parameters were the same as used in Fig. 5.

values for $\alpha[X_0]$, denoted α[GP4f]. The arrow at A(HAb2)/A(GP4f) = 40 shows which value is required by the data of Melikyan et al. (1995) fitted in Fig. 1 and Table 1. For the case of $\alpha[X_0(\text{GP4f})] = 0.05$, the vertical arrow shows that the minimal aggregate size is 6 HAs, but there are only N_ω(GP4f) = 0.7 fusogenic aggregates, which obviously will not fit the data. Thus, $\alpha[X_0(\text{GP4f})] > 0.05$. For α[GP4f] = 0.5, the estimate of the minimal aggregate size increases up to about 10, and the estimated number of HAs in fusogenic aggregates is about 10, which only gives a plausible fit to the fusion data (not shown). For α[GP4f] = 5, the estimate of the minimal aggregate size increases up to about 26, but the estimated number of fusogenic aggregates is reduced to about N_ω(GP4f) = 7, so the fit is worse. Overall, this model with $\beta = 0$ and a ratio of HA surface densities of 1.9 does permit an adequate (but not best) fit to the data, but the hybrid model produces best fits and is more to represent HA aggregation.

APPENDIX B. HA AGGREGATION RATE-LIMITED FUSION

The question here is whether the surface aggregation of HA trimers could be rate limiting to the fusion process. The simplest version of this kinetic model would assume that those HAs that have undergone the essential conformational change, denoted *Xe* here, proceed to aggregate to the ωmer, which then forms the first fusion pore. Aggregation of HAs that have not undergone the transformation would be irrelevant. This HA aggregation rate-limited model for fusion is

$$X \xrightarrow{k_f} Xe$$

$$Xe + Xe \xrightarrow{C_{11}} Xe_2$$

$$Xe_i + Xe_j \xrightarrow{C_{ij}} Xe_{j+i} \tag{B1}$$

$$Xe_\omega \xrightarrow{k_p} \text{FP}.$$

Xe_i denotes a surface aggregate of i transformed HA trimers. Such a model can show behavior similar to that developed for the model in the text, given the use of enough parameters. However, the basic structure of this kinetic model does not fit the data of Melikyan et al. (1995). To see this, we will consider the simplest case where all of the $C_{ij} = C$ rate constants are set equal and the rate of transformation to the essential conformation is rapid compared with the aggregation kinetics, $k_f \gg C[Xe_0]$. As shown in Bentz and Nir (1981a,b), this yields the classical Smoluchowski rate equations for aggregation, assuming, as was done in the text, that the loss of HA aggregates to the first fusion pore is insignificant because only the first one is being monitored,

$$[Xe_j] = [Xe_0]\frac{(C[Xe_0]t)^{j-1}}{(1 + C[Xe_0]t)^{j+1}}, \tag{B2}$$

for $j < \omega$. Following the path used for the model presented in the text, we assume that the formation of the first fusion pore is rate limited by the formation of the minimally sized ωmer aggregate, i.e., k_p is large, as in Eq. 7,

$$\begin{aligned}[Xe_\omega(t)] &= Ce^{-k_p t}\int_0^t e^{-k_p s}\sum_{j=1}^{\omega-1}[Xe_{\omega-j}(s)][Xe_j(s)]\,ds \\ &= C[Xe_0]^2(\omega-1)e^{-k_p t}\int_0^t e^{k_p s}\left[\frac{(C[Xe_0]s)^{\omega-2}}{(1 + C[Xe_0]s)^{\omega+2}}\right]ds,\end{aligned} \tag{B3}$$

$$\begin{aligned}[\text{FP}(t)] &= k_p\int_0^t Xe_\omega(s)\,ds \\ &\approx C[Xe_0]^2(\omega-1)\int_0^t \frac{(C[Xe_0]s)^{\omega-2}}{(1 + C[Xe_0]s)^{\omega+2}}\,ds \\ &\approx [Xe_0](C[Xe_0]t)^{\omega-1},\end{aligned}$$

where the order of the integrations were reversed and the last approximation assumes for the first fusion pore $C[Xe_0]t \ll 1$, similar to the model derived in the text. This means that the predicted initial fitted cumulant for cells having a first fusion pore, i.e., Eq. 4, when aggregation of HAs is rate limiting to fusion (denoted ARL) would be given by

$$Np,\ \text{ARL}(t) = 1 - \exp\{-A_{\text{ARL}}t^{\omega-1}\} \tag{B4}$$

$$A_{\text{ARL}} \equiv \delta\frac{(C[Xe_0])^\omega}{C}.$$

This equation has the same functional form as Eq. 8 in the text when $k_f t \ll 1$:

$$Np(t) \xrightarrow{k_f t << 1} 1 - \exp\{-(Ak_f^{q+1})t^{q+1}\}. \tag{B5}$$

In this limit, it is clear why the fitting to the data in Fig. 1 should show a strong correlation between k_f and the amplitude factors A(GP4f) and A(HAb2), because Ak_f^{q+1} equals some constant to fit the data. Clearly the fitted value of $k_f < 2 \times 10^{-4}\ s^{-1}$ largely satisfies the criteria of $k_f t \ll 1$ for the time scale of the formation of the first fusion pore.

Returning to the comparison of the two kinetic models, it is obvious that they have the same functional form initially, with differently interpreted parameters, e.g., $\omega - 1$ instead of $q + 1$. If Eq. B4 is used to fit the data of Fig. 1, we would obtain $\omega = 3.9 \pm 0.1$, because that was the fit obtained for $q + 1$ using Eq. 8, which is about equal to Eq. B5. Values for A_{ARL}(GP4f) and A_{ARL}(HAb2) can be obtained that fit either of these two curves as well as Eq. 8 did, but not both, because

$$\begin{aligned}\frac{A_{\text{ARL}}(\text{HAb2})}{A_{\text{ARL}}(\text{GP4f})} &= \left(\frac{\delta(\text{HAb2})}{\delta(\text{GP4f})}\right)\left(\frac{[\text{HAb2}]}{[\text{GP4f}]}\right)^\omega \\ &= 1.4(1.6)^{3.9} = 8.8 \ll 40.\end{aligned} \tag{B6}$$

That is, the ratio of the aggregation rate-limited amplitude factors cannot exceed the ratio of the HA cell surface densities raised to the power of ω, which must be only 3.9 to match the power dependence on the time t. Thus, although the HA aggregation rate-limited fusion kinetic model could fit either data set of Melikyan et al. (1995) in Fig. 1, it cannot fit both sets

simultaneously with self-consistent parameters in Eq. B5, because the required ratio of the amplitude factors is 40, not 8.8.

The kinetic model proposed in the text, with rapid HA aggregation and fusion rate limited by the essential conformational change of HA fits the data much better because it separates the HA surface dependence of fusogenic aggregate formation from the number of HAs that actually have to transform to create the fusion intermediate.

Obviously, assumptions have been made to permit simple analytical equations to be presented. However, most of these assumptions would have a small quantitative impact on the inability of the HA aggregation rate-limited fusion kinetic model to provide the correct differential HA surface density dependence on the first fusion pore formation. For example, to have the rate constant of the fusion pore formation, k_p, smaller would not significantly change the ratio of the amplitude factors in Eq. B6 because both A_{ARL}(GP4f) and A_{ARL}(HAb2) would be reduced by roughly the same amount. Using the Smoluchowski solutions for higher order aggregates is not exact, but, as shown in Bentz and Nir (1981a,b), these equations rather accurately reflect the behavior of the exact mass action equations very well, with suitable scaling of the value of C, and this scaling would be roughly equal for both of the amplitude factors.

Now, if the rate constant for first fusion pore formation, k_p, were slow compared with the rate of HA aggregation, then the kinetics described in the text would be recovered, because there is no clear reason to exclude the aggregation of untransformed HAs with those that have undergone the essential conformational change. This would yield aggregates of HA, some of which have achieved the essential conformational change, just as described in the text. Although many types of HA aggregation could be postulated, there is no evidence that any type except rapid equilibration prior to fusion is relevant.

In contrast, it must be clear that this Appendix is showing only that the basic structure of the HA aggregation rate-limited fusion kinetic model does not fit the data of Melikyan et al. (1995). Given the number of parameters in Eq. B1, beyond the minimal set used, it is certain that values could be chosen that would allow reasonable fittings of the data in Fig. 1. But this would require extra assumptions, whose purpose is only to fit the very first data set available. To elucidate how HA actually induces fusion subsequent to the exposure of the fusion peptide will require the analysis of many sets of data, so it is best to begin with the most robust model. Thus, the leading kinetic model is that, following low pH treatment, there is rapid exposure of the fusion peptide followed by rapid aggregation of HAs, followed by a slow essential conformational change of some of these HAs leading to the first fusion pore. Plonsky et al. (1999) suggested that the aggregation of the baculovirus fusion protein GP64 was not rate limiting for fusion pore formation.

I wish to thank Dr. Michael O'Connor for many useful discussions about data fitting, help with the MATLAB programming and for critically reading the final manuscript. I would also like to thank Drs. Leonid Chernomordik, Harma Ellens, Grigory Melikyan, and David Siegel for critically reading the original manuscript.

REFERENCES

Alford, D., H. Ellens, and J. Bentz. 1994. Fusion of influenza virus with sialic acid-bearing target membranes. *Biochemistry.* 33:1977–1987.

Bentz, J. 1992. Intermediates and kinetics of membrane fusion. *Biophys. J.* 63:448–459.

Bentz, J. 1993. Viral Fusion Mechanisms. CRC Press, Boca Raton, FL.

Bentz, J. 2000. Membrane fusion mediated by coiled coils: a hypothesis. *Biophys. J.* 76:A438.

Bentz, J., and S. Nir. 1981a. Aggregation of colloidal particles modeled as a dynamical process. *Proc. Natl. Acad. Sci. USA.* 78:1634–1637.

Bentz, J., and S. Nir. 1981b. Mass action kinetics and equilibria of reversible aggregation. *J. Chem. Soc. Faraday Trans. I.* 77:1249–1275.

Bentz, J., D. Covell, and S. Nir. 1988. Mass action kinetics of virus–cell aggregation and fusion. *Biophys. J.* 54:449–462.

Bentz, J., H. Ellens, and D. Alford. 1990. An architecture for the fusion site of influenza hemagglutinin. *FEBS Lett.* 276:1–5.

Blumenthal, R., D. P. Sarkar, S. Durell, D. E. Howard, and S. J. Morris. 1996. Dilation of the influenza hemagglutinin fusion pore revealed by the kinetics of individual fusion events. *J. Cell Biol.* 135:63–71.

Brandon, C., and J. Tooze. 1991. Introduction to Protein Structure. Garland, New York.

Brunner, J., and M. Tsuredome. 1993. Fusion–protein membrane interactions as studied by hydrophobic photolabelling. *In* Viral Fusion Mechanisms. J. Bentz, editor. CRC Press, Boca Raton, FL. 67–84.

Bullough, P. A., F. M. Hughson, J. J. Skehel, and D. C. Wiley. 1994. Structure of influenza haemagglutinin at the pH of membrane fusion. *Nature.* 371:37–43.

Carr, C. M., and P. S. Kim. 1993. A spring-loaded mechanism for the conformational change in influenza hemagglutinin. *Cell.* 73:823–832.

Carr, C. M., C. Chaudhry, and P. S. Kim. 1997. Influenza hemagglutinin is a spring-loaded by a metastable native configuration. *Proc. Nat. Acad. Sci. USA.* 94:14306–14313.

Chen, J., S. Wharton, W. Weissenhorn, L. Calder, F. Hughson, J. J. Skehel, and D. C. Wiley. 1995. A soluble domain of the membrane-anchoring chain of influenza virus hemagglutinin (HA2) folds in *Escherichia coli* into the low pH induced conformation. *Proc. Natl. Acad. Sci. USA.* 92:12205–12209.

Chernomordik, L. V., E. Leikina, V. Frolov, P. Bronk, and J. Zimmerberg. 1997. An early stage of membrane fusion mediated by the low pH conformation of influenza hemagglutinin depends upon membrane lipids. *J. Cell. Biol.* 136:81–93.

Chernomordik, L. V., V. A. Frolov, E. Leikina, P. Bronk, and J. Zimmerberg. 1998. The pathway of membrane fusion catalyzed by influenza hemagglutinin: restriction of lipids, hemifusion, and lipidic fusion pore formation. *J. Cell. Biol.* 140:1369–1382.

Chernomordik, L. V., E. Leikina, M. M. Kozlov, V. A. Frolov, and J. Zimmerberg. 1999. Structural intermediates in influenza hemagglutinin-mediated fusion. *Mol. Membr. Biol.* 16:33–42.

Danieli, T., S. L. Pelletier, Y. I. Henis, and J. M. White. 1996. Membrane fusion mediated by the influenza virus hemagglutinin requires the concerted action of at least three hemagglutinin trimers. *J. Cell Biol.* 133:559–569.

Dieckmann, G. R., D. McRorie, J. Lear, K. Sharp, W. F. DeGrado, and V. Pecoraro. 1998. The role of protonation and metal chelation preferences in defining the properties of mercury-binding coiled coils. *J. Mol. Biol.* 280:897–912.

Durell, S., I. Martin, J.-M. Ruysschaert, Y. Shai, and R. Blumenthal. 1997. What studies of fusion peptides tell us about viral envelope glycoprotein-mediated membrane fusion. *Mol. Membr. Biol.* 14:97–112.

Ellens, H., J. Bentz, D. Mason, F. Zhang, and J. M. White. 1990. Fusion of influenza hemagglutinin-expressing fibroblasts with glycophorin-bearing liposomes: role of hemagglutinin surface density. *Biochemistry.* 29:9697–9707.

Epand, R. F., J. C. Macosko, C. J. Russell, Y. K. Shin, and R. M. Epand. 1999. The ectodomain of HA2 of influenza virus promotes rapid pH dependent membrane fusion. *J. Mol. Biol.* 286:489–503.

Gaudin, Y., R. W. Ruigrok, and J. Brunner. 1995. Low-pH induced conformational changes in viral fusion proteins: implications for the fusion mechanism. *J. Gen. Virol.* 76:1541–1556.

Godley, L., J. Pfeifer, D. Steinhauer, B. Ely, G. Shaw, R. Kaufmann, E. Suchanek, C. Pabo, J. J. Skehel, D. C. Wiley, and S. Wharton. 1992. Introduction of intersubunit disulfide bonds in the membrane-distal region of the influenza hemagglutinin abolishes membrane fusion activity. *Cell.* 68:635–645.

Gray, C., and L. K. Tamm. 1997. Structural studies on membrane-embedded influenza hemagglutinin and its fragments. *Protein Sci.* 6:1993–2006.

Gray, C., and L. K. Tamm. 1998. pH-induced conformational changes of membrane-bound influenza hemagglutinin and its effect on target lipid bilayers. *Protein Sci.* 7:2359–2373.

Hernandez, L. D., L. R. Hoffman, T. G. Wolfsberg, and J. M. White. 1996. Virus–cell and cell–cell fusion. *Ann. Rev. Cell Dev. Biol.* 12:627–661.

Körte, T., K. Ludwig, M. Krumbiegel, D. Zirwer, G. Damaschun, and A. Herrmann. 1997. Transient changes of the conformation of hemagglutinin of influenza virus at low pH detected by time-resolved circular dichroism spectroscopy. *J. Biol. Chem.* 272:9764–9770.

Körte, T., K. Ludwig, F. P. Booy, R. Blumenthal, and A. Herrmann. 1999. Conformational intermediates and fusion activity of influenza virus hemagglutinin. *J. Virol.* 73:4567–4574.

Kozlov, M. M., and L. V. Chernomordik. 1998. A mechanism of protein-mediated fusion: coupling between refolding of the influenza hemagglutinin and lipid rearrangements. *Biophys. J.* 75:1384–1396.

Markovic, I., H. Pulyaeva, A. Sokoloff, and L. V. Chernomordik. 1998. Membrane fusion mediated by baculovirus gp64 involves assembly of stable gp64 trimers into multiprotein aggregates. *J. Cell. Biol.* 143: 1155–1166.

Melikyan, G. B., W. Niles, and F. S. Cohen. 1995. The fusion kinetics of influenza hemagglutinin expressing cells to planar bilayer membranes is affected by HA surface density and host cell surface. *J. Gen. Physiol.* 106:783–802.

Molski, A., S. Berling, and J. Keizer. 1996. Rapid chemical reactions in two dimensions: spatially nonlocal effects. *J. Phys. Chem.* 100: 19049–19054.

Pak, C. C., M. Krumbiegel, and R. Blumenthal. 1994. Intermediates in influenza virus PR/8 haemagglutinin-induced membrane fusion. *J. Gen. Virol.* 75:395–399.

Plonsky, I., M. S. Cho, A. G. Oomens, G. Blissard, and J. Zimmerberg. 1999. An analysis of the role of the target membrane on the Gp64-induced fusion pore. *Virology.* 253:65–76.

Puri, A., F. P. Booy, R. W. Doms, J. M. White, and R. Blumenthal. 1990. Conformational changes and fusion activity of influenza virus hemagglutinin of the H2 and H3 subtypes: effects of acid pretreatment. *J. Virol.* 64:3824–3832.

Qiao, H., S. Pelletier, L. Hoffman, J. Hacker, R. Armstrong, and J. M. White. 1998. Specific single or double proline substitutions in the "spring-loaded" coiled coil region of the influenza hemagglutinin impair or abolish membrane fusion activity. *J. Cell Biol.* 141:1335–1347.

Razinkov, V. I., G. B. Melikyan, R. M. Epand, R. F. Epand, and F. S. Cohen. 1998. Effects of spontaneous bilayer curvature on influenza virus-mediated fusion pores. *J. Gen. Physiol.* 112:409–422.

Razinkov, V. I., G. B. Melikyan, and F. S. Cohen. 1999. Lipid continuity between cells expressing hemagglutinin (HA) from influenza virus and planar bilayer membranes can precede the formation of fusion pores that fully enlarge. *Biophys. J.* 76:A437.

Ruigrok, R. W. H., A. Aitken, L. J. Calder, S. R. Martin, J. J. Skehel, S. A. Wharton, W. Weis, and D. C. Wiley. 1988. Studies on the structure of the influenza virus hemagglutinin at the pH of membrane fusion. *J. Gen. Virol.* 69:2785–2795.

Shangguan, T., D. Alford, and J. Bentz. 1996. Influenza virus-liposomes lipid mixing is leaky and largely insensitive to the material properties of the target membrane. *Biochemistry.* 35:4956–4965.

Shangguan, T., D. Siegel, J. Lear, P. Axelsen, D. Alford, and J. Bentz. 1998. Morphological changes and fusogenic activity of influenza virus hemagglutinin. *Biophys. J.* 74:54–62.

Skehel, J. J., P. M. Bayley, E. B. Brown, S. R. Martin, M. D. Waterfield, J. M. White, I. A. Wilson, and D. C. Wiley. 1982. Changes in the conformation of influenza virus hemagglutinin at the pH optimum of virus-mediated membrane fusion. *Proc. Natl. Acad. Sci. USA.* 79: 968–972.

Skehel, J. J., and D. C. Wiley. 1998. Coiled coils in both intracellular vesicle and viral membrane fusion. *Cell.* 95:871–874.

Sosnick, T. R., S. Jackson, R. R. Wilk, S. W. Englander, and W. F. DeGrado. 1996. The role of helix formation in the folding of a fully alpha-helical coiled coil. *Proteins.* 24:427–432.

Stegmann, T., J. M. White, and A. Helenius. 1990. Intermediates in influenza induced membrane fusion. *EMBO J.* 13:4231–4241.

Stegmann, T., and A. Helenius. 1993. Influenza virus fusion: from models toward a mechanism. *In* Viral Fusion Mechanisms. J. Bentz, editor. CRC Press, Boca Raton, FL. 89–113.

Steinhauer, D. A., J. Martin, Y. P. Lin, S. A. Wharton, M. B. A. Oldstone, J. J. Skehel, and D. C. Wiley. 1996. Studies using double mutants of the conformational transitions in influenza hemagglutinin required for its membrane fusion activity. *Proc. Natl. Acad. Sci. USA.* 93:12873–12878.

Torney, D. C., and H. McConnell. 1983. Diffusion-limited reaction rate theory for two dimensional systems. *Proc. R. Soc. Lond.* A387:147–170.

Tse, F. W., A. Iwata, and W. Almers. 1993. Membrane flux through the pore formed by a fusogenic viral envelope protein during cell fusion. *J. Cell Biol.* 121:543–552.

Weissenhorn, W., A. Dessen, L. J. Calder, S. C. Harrison, J. J. Skehel, and D. C. Wiley. 1999. Structural basis for membrane fusion by enveloped viruses. *Mol. Membr. Biol.* 16:3–9.

Wharton, S. A., L. J. Calder, R. W. H. Ruigrok, J. J. Skehel, D. A. Steinhauer, and D. C. Wiley. 1995. Electron microscopy of antibody complexes of influenza virus hemagglutinin in the fusion pH conformation. *EMBO J.* 14:240–246.

White, J., and I. A. Wilson. 1987. Anti-peptide antibodies detect steps in a protein conformational change: low-pH activation of the influenza virus hemagglutinin. *J. Cell Biol.* 105:2887–2896.

Wilson, I. A., J. J. Skehel, and D. C. Wiley. 1981. Structure of the haemagglutinin membrane glycoprotein of influenza virus at 3 Å resolution. *Nature.* 289:366–373.

Yu, Y. G., D. S. King, and Y.-K. Shin. 1994. Insertion of a coiled-coil peptide from influenza virus hemagglutinin into membranes. *Science.* 266:274–276.

Zimmerberg, J., R. Blumenthal, D. P. Sarkar, M. Curran, and S. J. Morris. 1994. Restricted movement of lipid and aqueous dyes through pores formed by influenza hemagglutinin during cell fusion. *J. Cell Biol.* 127:1885–1894.